

## Inter-model comparison of global hydroxyl radical (OH) distributions and their impact on atmospheric methane over the 2000-2016 period

Yuanhong Zhao<sup>1</sup>, Marielle Saunois<sup>1</sup>, Philippe Bousquet<sup>1</sup>, Xin Lin<sup>1\*</sup>, Antoine Berchet<sup>1</sup>, Michaela I.  
5 Hegglin<sup>2</sup>, Josep G. Canadell<sup>3</sup>, Robert B. Jackson<sup>4</sup>, Didier A. Hauglustaine<sup>1</sup>, Sophie Szopa<sup>1</sup>, Ann R.  
Stavert<sup>5</sup>, Nathan Luke Abraham<sup>6, 7</sup>, Alex T. Archibald<sup>6, 7</sup>, Slimane Bekki<sup>8</sup>, Makoto Deushi<sup>9</sup>, Patrick  
Jöckel<sup>10</sup>, B atrice Josse<sup>11</sup>, Douglas Kinnison<sup>12</sup>, Ole Kirner<sup>13</sup>, Virginie Mar cal<sup>11</sup>, Fiona M. O'Connor<sup>14</sup>,  
David A. Plummer<sup>15</sup>, Laura E. Revell<sup>16, 17</sup>, Eugene Rozanov<sup>16, 18</sup>, Andrea Stenke<sup>16</sup>, Sarah Strode<sup>19, 20</sup>,  
Simone Tilmes<sup>21</sup>, Edward J. Dlugokencky<sup>22</sup>, and Bo Zheng<sup>1</sup>

10

<sup>1</sup> Laboratoire des Sciences du Climat et de l'Environnement, LSCE-IPSL (CEA-CNRS-UVSQ),  
Universit Paris-Saclay, 91191 Gif-sur-Yvette, France

<sup>2</sup> Department of Meteorology, University of Reading, Earley Gate, Reading RG6 6BB, United Kingdom

<sup>3</sup> Global Carbon Project, CSIRO Oceans and Atmosphere, Canberra, Australian Capital Territory 2601,  
15 Australia

<sup>4</sup> Earth System Science Department, Woods Institute for the Environment, and Precourt Institute for  
Energy, Stanford University, Stanford, CA 94305, USA

<sup>5</sup> CSIRO Oceans and Atmosphere, Aspendale, Victoria, 3195, Australia

<sup>6</sup> Department of Chemistry, University of Cambridge, CB2 1EW, UK

20 <sup>7</sup> NCAS-Climate, University of Cambridge, CB2 1EW, UK

<sup>8</sup> LATMOS, Universit Pierre et Marie Curie, 4 Place Jussieu Tour 45, couloir 45-46, 3e  tage Boite 102,  
75252, Paris Cedex 05, France

<sup>9</sup> Meteorological Research Institute, 1-1 Nagamine, Tsukuba, Ibaraki, 305-0052, Japan

<sup>10</sup> Deutsches Zentrum f r Luft- und Raumfahrt (DLR), Institut f r Physik der Atmosph re,  
25 Oberpfaffenhofen, Germany

<sup>11</sup>Centre National de Recherches Météorologiques, Université de Toulouse, Météo-France, CNRS, Toulouse, France

<sup>12</sup>Atmospheric Chemistry Observations and Modeling Laboratory, National Center for Atmospheric Research, 3090 Center Green Drive, Boulder, CO, 80301, USA

30 <sup>13</sup> Steinbuch Centre for Computing, Karlsruhe Institute of Technology, Karlsruhe, Germany

<sup>14</sup> Met Office Hadley Centre, Exeter, EX1 3PB, UK

<sup>15</sup> Climate Research Branch, Environment and Climate Change Canada, Montréal, Canada

<sup>16</sup> Institute for Atmospheric and Climate Science, ETH Zürich (ETHZ), Zürich, Switzerland

<sup>17</sup> School of Physical and Chemical Sciences, University of Canterbury, Christchurch, New Zealand

35 <sup>18</sup> Physikalisch-Meteorologisches Observatorium Davos World Radiation Centre, Dorfstrasse 33, 7260 Davos Dorf

<sup>19</sup> NASA Goddard Space Flight Center, Greenbelt, MD, USA

<sup>20</sup> Universities Space Research Association (USRA), GESTAR, Columbia, MD, USA

<sup>21</sup> National Center for Atmospheric Research, Boulder, CO, USA

40 <sup>22</sup> Global Monitoring Division, NOAA Earth System Research Laboratory, Boulder, CO, USA

\* Now at: Climate and Space Sciences and Engineering, University of Michigan, Ann Arbor, MI 48109, USA

45 *Correspondence to:* Yuanhong Zhao (yuanhong.zhao@lsce.ipsl.fr)

## Abstract

The modeling study presented here aims to estimate how uncertainties in global hydroxyl radical (OH) distributions, variability, and trends may contribute to resolve discrepancies between simulated and observed methane (CH<sub>4</sub>) changes since 2000. A multi-model ensemble of 14 OH fields were analysed and were aggregated into 64 scenarios to force the offline atmospheric chemistry transport model LMDz with a standard CH<sub>4</sub> emission scenario over the period 2000-2016. The multi-model simulated global volume-weighted tropospheric mean OH concentration([OH]) averaged over 2000-2010 ranges between  $8.7 \times 10^5$  and  $12.8 \times 10^5$  molec cm<sup>-3</sup>. The inter-model differences in tropospheric OH burden and vertical distributions are mainly determined by the differences in the nitrogen oxide (NO) distributions, while the spatial discrepancies between OH fields are mostly due to differences in natural emissions and VOC chemistry. From 2000 to 2010, most simulated OH fields show an increase of  $0.1-0.3 \times 10^5$  molec cm<sup>-3</sup> in the tropospheric mean [OH], with year-to-year variations much smaller than during the historical period 1960-2000. Once ingested into the LMDz model, these OH changes translated into a 5 to 15 ppbv reduction in CH<sub>4</sub> mixing ratio in 2010, which represent 7%-20% of the model simulated CH<sub>4</sub> increase due to surface emissions. Between 2010 and 2016, the ensemble of simulations showed that OH changes could lead to a CH<sub>4</sub> mixing ratio uncertainty of  $> \pm 30$  ppbv. Over the full 2000-2016 time period, using a common state-of-the-art but non-optimized emission scenario, the impact of [OH] changes tested here can explain up to 54% of the gap between model simulations and observations. This result emphasizes the importance of better representing OH abundance and variations in CH<sub>4</sub> forward simulations and emission optimizations performed by atmospheric inversions.

## 1 Introduction

70 The hydroxyl radical (OH) is the main oxidizing agent in the troposphere (Levy, 1971). OH is produced by the reaction of water vapor with excited oxygen atoms ( $O(^1D)$ ), produced by ozone ( $O_3$ ) photolysis ( $\lambda < 340\text{nm}$ ). In the troposphere, OH is rapidly removed by reactions with carbon monoxide (CO), methane ( $CH_4$ ) and non-methane volatile organic compounds (NMVOCs) to generate hydroperoxyl radical ( $HO_2$ ) or organic peroxy radicals ( $RO_2$ ), resulting in a short lifetime of a few seconds (Logan et al., 1981; 75 Lelieveld et al., 2004).  $HO_2$  and  $RO_2$  can further react with nitrogen oxide (NO) to regenerate OH (Crutzen, 1973; Zimmerman et al., 1987). At high latitudes, such a secondary production plays an important role, because the OH primary production is limited by the supply of  $O(^1D)$  and water vapor (Spivakovsky et al., 2000). The abundance of OH reflects the combined effects of atmospheric composition (tropospheric  $O_3$ , and NO, CO,  $CH_4$ , and NMVOCs) and of meteorological factors such as humidity, UV radiation, and 80 temperature.

Due to its short lifetime, global [OH] is difficult to estimate from direct measurements. Current understanding on global [OH] has been obtained either from inversion of 1-1-1trichloroethane (methyl chloroform, MCF) (Prinn et al., 2005; Bousquet et al., 2005; Montzka et al., 2011; Rigby et al., 2017; 85 Turner et al., 2017), or using atmospheric chemistry models (Naik et al., 2013; Voulgarakis et al., 2013, Lelieveld et al., 2016). The former approach relies on the fact that OH is the main sink of MCF and on the hypotheses that emissions and concentrations of MCF are well known and well measured, respectively. The latter approach relies on chemistry-transport modeling with chemistry schemes of varying complexity. The global mass-weighted tropospheric mean [OH] in the 2000s calculated by atmospheric chemistry 90 models was found to be about  $11.5 \times 10^5 \text{ molec cm}^{-3}$ , with an inter-model dispersion of  $\pm 15\%$  (Naik et al., 2013; Voulgarakis et al., 2013). Atmospheric chemistry models usually calculate higher [OH] over the Northern hemisphere than the Southern hemisphere (N/S ratio  $> 1$ ) (Naik et al., 2013) whereas MCF and  $^{14}CO$  observations indicate a N/S ratio slightly smaller than 1 (Brenninkmeijer et al., 1992; Bousquet et

al., 2005; Patra et al., 2014).

95

OH determines the lifetime of most pollutants and non-CO<sub>2</sub> greenhouse gases including CH<sub>4</sub>, the second most important anthropogenic greenhouse gas after carbon dioxide (CO<sub>2</sub>) (Ciais et al., 2013). About 90% of tropospheric CH<sub>4</sub> is removed by reacting with OH (Ehhalt et al., 1974; Kirschke et al., 2013; Saunio et al., 2016). The tropospheric CH<sub>4</sub> chemical lifetime against OH oxidation (global annual mean atmospheric CH<sub>4</sub> burden divided by annual CH<sub>4</sub> tropospheric loss by OH) calculated by the models that participated in the Atmospheric Chemistry and Climate Model Inter-comparison Project (ACCMIP) is 9.3±1.6 years, and the CH<sub>4</sub> total lifetime including all sink processes is 8.3±0.8 years (Naik et al., 2013; Voulgarakis et al., 2013), smaller than that of 9.1±0.9 years lifetime constrained by observations (Prather et al., 2012).

105

The tropospheric CH<sub>4</sub> burden has more than doubled compared to the pre-industrial era due to anthropogenic activities and climate change, resulting in about 0.62 W m<sup>-2</sup> additional radiative forcing (Etminan et al., 2016). The global mean CH<sub>4</sub> growth rate decreased to near zero in the early 2000s but resumed increasing at ~5ppbv yr<sup>-1</sup> since 2006 and reached more than 10 ppbv yr<sup>-1</sup> in 2014 and in 2018 (Ed Dlugokencky, NOAA/ESRL, 2019). The growth rate of CH<sub>4</sub> is determined by the imbalance of its sources, primarily from anthropogenic activities (agriculture, waste, fossil fuel production and usage, and biomass burning) but also from natural emissions (mainly wetland and other inland waters), and sinks (OH oxidation, other chemical reactions with chlorine and oxygen radicals, and soil uptake). The precise reasons for the stagnation and renewed CH<sub>4</sub> growths still remain unclear (e.g. Rigby et al 2017; Saunio et al., 2017; Nisbet et al., 2019; Turner et al., 2019).

115

Several studies have linked such CH<sub>4</sub> variations to inter-annual variations and trend of OH. Based on MCF inversions, McNorton et al. (2016) concluded that an increase in [OH] significantly contributed to

the stable atmospheric CH<sub>4</sub> before 2007; Rigby et al. (2008) found that a decrease of  $4 \pm 14\%$  in [OH] could partly explain the CH<sub>4</sub> growth between 2006 and 2007. Bousquet et al. (2011) found a smaller decrease in [OH] (<1% over the two years) and attributed the increase in CH<sub>4</sub> mostly to enhanced emissions over tropical regions; Montzka et al. (2011) also calculated a small inter-annual variation of  $2.3 \pm 1.5\%$  in [OH] during 1998 to 2007. More recently, based on multi-species box model inversions, Rigby et al. (2017) and Turner et al. (2017) inferred a decrease of  $8 \pm 11\%$  and 7% in [OH] during 2004-2014 and 2003-2016 respectively. Both of these studies suggested that such a decrease in [OH] is equivalent to an increase of more than 20 Tg yr<sup>-1</sup> in CH<sub>4</sub> emissions, and therefore could significantly contribute to explain the post-2007 CH<sub>4</sub> atmospheric growth, although a solution with constant OH cannot be discarded. Meanwhile, not only the OH trend calculated by atmospheric chemistry models cannot reach consensus, but it can also be different from the OH trend inferred by top-down approaches from observations. Indeed, Dalsøren et al. (2016) simulated ~ 8% increase in OH during 1970 to 2012, while other models mostly calculated only a small increase of [OH] (decrease in CH<sub>4</sub> lifetime) or no trend in [OH] from 1980s to 2000s (e.g. Voulgarakis et al., 2013; Nicely et al., 2018). Top-down observation-constrained approaches (e.g. Rigby et al., 2017) tend to find flat to decreasing OH trend over this period but with larger year-to-year variations than models. The discrepancy between individual process-based models and MCF-proxy approaches, and the uncertainties, limit our ability to be conclusive on the role of [OH] changes to explain the CH<sub>4</sub> changes over the past decades.

To better understand OH distributions, trends, and influences on CH<sub>4</sub> since 2000, we have performed an inter-model comparison of 14 OH fields, including 11 derived from chemistry transport and chemistry-climate models that took part in the phase 1 of the Chemistry-Climate Model Initiative (CCMI) (Hegglin and Lamarque, 2015; Morgenstern et al., 2017), 2 from different configurations of the LSCE atmospheric chemistry transport model LMDz-INCA (Hauglustaine et al., 2004; Szopa et al., 2013), and 1 from the TRANSCOM 2011 inter-comparison exercise (Patra et al., 2011). We then conducted an ensemble of CH<sub>4</sub>

simulations with different OH fields using the LMDz chemistry-transport model to estimate a range for  
145 the contribution of changes in [OH] to the atmospheric CH<sub>4</sub> mixing ratio changes since 2000, and to relate  
this contribution to spatio-temporal characteristics of the different OH fields. Year-to-year integrations of  
CCMI and INCA models driven by time-varying emissions and meteorology facilitate the investigation  
of interannual variability in OH, which was not possible using the ACCMIP time-slice simulations. In the  
following, our analysis first provides a brief description of the OH fields used in this study and the LMDz  
150 offline model (section 2). Section 3 compares the OH fields, analyses the factors contributing to inter-  
model differences and presents their inter-annual variability. Section 4 presents and discusses the impact  
of the different OH fields on the global CH<sub>4</sub> burden and growth rates simulated by LMDz. Section 5  
summarizes the results and conclusion.

## 155 **2 Method**

### **2.1 OH fields**

The CCMI project aims to conduct a detailed evaluation of atmospheric chemistry models in order to  
assess uncertainties in the models' projections of various climate-related topics such as tropospheric  
160 composition (Hegglin and Lamarque, 2015; Morgenstern et al., 2017). The CCMI OH fields used in our  
study are obtained from 10 different models and 3 CCMI reference experiments: REF-C1 (covering the  
time period 1960-2010), REF-C2 (covering 1960-2100), and REF-C1SD (1980-2010). The REF-C1  
experiment is driven by state-of-the-art historical forcings and sea surface temperatures (sst) and sea ice  
concentrations (sic) based on observations, while the REF-C2 experiment is using either coupled ocean  
165 and sea ice modules or prescribes sst and sic obtained from another climate model. Since the REF-C1  
experiment is supposed to be more realistic regarding sea surface conditions, our analysis focused on OH  
fields from the REF-C1 experiment before 2010 and only tested the influences of OH on CH<sub>4</sub> simulations  
after 2010 by applying the inter-annual variability from the REF-C2 experiment. The models of REF-

C1SD experiment are nudged towards reanalysis datasets. The REF-C1SD experiment is not analyzed in  
170 the main text since it has been conducted by only part of the models and covers a shorter time period. A  
comparison of spatial and vertical distributions of OH fields from REF-C1 experiment with that from  
REF-C1SD reveals only small latitudinal differences (<10%, see Section S1). Detailed descriptions of  
CCMI simulations can be found in Morgenstern et al. (2017).

175 In this study, we used only the CCMI models that include detailed tropospheric ozone chemistry as listed  
in Table 1. Note that EMAC offers fields at two different model resolutions. The level of detail in chemical  
mechanism, in particular with respect to included NMVOCs, varies among the models. For example,  
CMAM does not include any NMVOC species, but added 250 Tg CO emissions to account for CO  
production from isoprene oxidation. UМУKCA-UCAM only include HCHO (formaldehyde) and  
180 SOCOL3 only include HCHO and C<sub>5</sub>H<sub>8</sub> (isoprene). Other models include multiple primary NMVOC  
species and more complex VOC chemistry.

The anthropogenic emissions recommended for the two CCMI reference simulations are the MACCity  
inventory (Granier et al., 2011) for 1960-2000. After 2000, the REF-C1 experiment continued to use the  
185 MACCity inventory (which follow the RCP8.5 inventory after 2000), while the REF-C2 used the RCP6.0  
inventory (Masui et al., 2011). The CMAM model did not follow this procedure and used the ACCMIP  
historical database of emissions (Lamarque et al., 2010) until 2000 followed by RCP8.5 emissions (Riahi  
et al., 2011) instead. Biomass burning emissions used in REF-C1 are RETRO inventory (Schultz et al.  
2008) before 1996 and GFEDv3 inventory (van der Werf et al., 2010) for 1997-2010 with interannual  
190 variability. CCMI model simulations also include natural emissions from lightning, soil and biogenic  
sources. Lightning NO<sub>x</sub> emissions are calculated based on meteorological data such as cloud top height  
(Price and Rind, 1994; Grewe et al., 2001) and updraft mass flux (Allen and Pickering, 2002). Soil NO<sub>x</sub>  
emissions are calculated interactively in EMAC and GEOSCCM using the scheme described by Yienger



and Levy (1995), but are prescribed in other models. Biogenic NMVOC emissions in CESM and  
195 GEOSCCM are calculated based on the distribution of plant functional types and meteorology conditions  
with MEGAN, whereas the other models apply prescribed biogenic NMVOC emissions.

The CCMi models do not represent CH<sub>4</sub> emissions explicitly but prescribe CH<sub>4</sub> surface mixing ratios vary  
in time according to the RCP6.0 scenario (global mean of ~1750ppbv averaged over 2000-2010) with  
200 different spatial distributions: GEOSCCM, CESM and EMAC models consider the full latitudinal  
gradient and prescribe CH<sub>4</sub> surface mixing ratios about 50 ppbv higher over the Northern hemisphere  
than over the Southern hemisphere; while CMAM, MRI-ESM1r1, and SOCOL3 use global uniform  
values. Photolysis rates are calculated either following online schemes such as FAST-JX (Neu et al., 2007;  
Telford et al., 2013) by GEOSCCM, HadGEM3-EA, UMUKA-UCAM, JVAL (Sander et al., 2014) by  
205 EMAC, or based on look-up tables with online cloud corrections by the rest of the models used in this  
study. Kinetics and photolysis data are mainly from Sander et al. (2011) with a few exceptions. More  
information on model characteristics can be found in Morgenstern et al. (2017) and references listed in  
Table 1.

210 Additionally to CCMi OH fields, we also included 2 OH fields simulated by the Interaction with  
Chemistry and Aerosols (INCA) coupled to the general circulation model of the Laboratoire de  
Météorologie Dynamique (LMD), LMDz (Sadourny and Laval, 1984; Hourdin and Armengaud, 1999;  
Hourdin et al., 2006; Hauglustaine et al., 2004). The two INCA simulations are driven by different  
versions of the LMDz GCM (INCA NMHC-AER-S covering time period 2000-2010 (Terrenoire et al.,  
215 2019), and INCA NMHC covering time period 2000-2009 (Szopa et al., 2013)), which provide different  
water vapor fields, and include different chemistry and emissions. The INCA NMHC-AER-S used the  
latest version of INCA model including both gas phase (NMHC) and aerosol (AER) chemistry in the  
troposphere and the stratosphere (S) (Terrenoire et al., 2019), while INCA NMHC used a former version

that only includes tropospheric gas-phase chemistry (Szopa et al., 2013). Anthropogenic emissions from  
220 Short-Lived Pollutants (ECLIPSE) inventory (Stohl et al., 2015) for 2005 and RCP 85 emission inventory  
(Riahi et al., 2011)) for 2010 are applied to every year of INCA NMHC-AER-S and INCA NMHC  
simulations, respectively.

Finally, we included in this study the OH field used in TransCom simulations, which results from a  
225 combination of the semi-empirical tropospheric 3-dimensional OH field from Spivakovsky et al. (2000)  
and a 2-dimensional simulated stratospheric OH for year 2000. The tropospheric OH was calculated using  
prescribed chemical species ( $O_3$ , nitrogen oxides, and CO) as well as meteorological fields (temperature,  
humidity, and cloud optical depth) to fit the observations. The original tropospheric [OH] has been  
reduced by 8% to match  $CH_3CCl_3$  observations (Patra et al., 2011). The TransCom OH field is only  
230 climatological (one year of monthly fields).

In total, we compared 14 OH fields: 11 from CCMI, 2 from the online LMDz-INCA model and 1 from  
TransCom. We analyzed spatial distributions and annual variations of OH fields by calculating volume-  
weighted tropospheric mean [OH] with tropopause pressure using WMO tropopause definition on 3D  
235 temperature for each model (World Meteorological Organization, 1957). Since employing different  
weightings can result in large differences in mean [OH] (Lawrence et al., 2001), we also calculated dry  
air mass-weighted tropospheric mean [OH] to better compare with previous studies.

## 2.2 LMDz model simulations

### 240 2.2.1 Model description and setup

We have run the offline version LMDz5B of the LMDz model (Locatelli et al., 2015) at a horizontal  
resolution of  $3.75^\circ \times 1.85^\circ$  with 39 vertical layers up to 3 hPa to assess the impact of OH on tropospheric  
CH<sub>4</sub>. All monthly mean OH fields have been interpolated to the LMDz model grid. The transport of

atmospheric tracers is driven by prescribed air mass fluxes provided by the general circulation model  
245 LMDz with horizontal wind fields nudged to ERA-Interim re-analysis meteorology data produced by the  
European Center for Medium-Range Weather Forecasts (Dee et al, 2011). The vertical transport is  
parameterized according to updates of the Emanuel (1991) scheme for convection and of the Louis (1979)  
scheme for boundary layer mixing (Hourdin et al., 2016; Locatelli et al., 2015). Chemistry module applied  
here is the simplified chemistry module SACS (Pison et al., 2009). Chemical sinks of CH<sub>4</sub> are calculated  
250 using prescribed three-dimensional OH and O(<sup>1</sup>D) fields, and variation in CH<sub>4</sub> cannot feedback on OH.  
No chlorine-related sink is simulated in this version of the model. To assess the influences of OH only,  
all LMDz simulations used the same O(<sup>1</sup>D) fields generated by INCA model simulations. The reaction rate  
coefficient (k) for CH<sub>4</sub> destruction by OH in the model is computed depending on temperature following  
Sander et al. (2011):

$$255 \quad k = 2.45 \times 10^{-12} e^{-1775 \times (\frac{1}{T})} \quad (1)$$

The LMDz model has been applied in various studies focusing on long-lived gases such as CH<sub>4</sub>, CO<sub>2</sub> and  
MCF (Bousquet et al., 2005; Pison et al., 2009; Lin et al., 2018). It has also been used in model inter-  
comparison projects such as the TransCom experiment (Patra et al., 2011) with the simplified chemistry  
module SACS (Pison et al., 2009) and CCMI (Morgenstern et al., 2017) but only with the stratospheric  
260 chemistry model PEPROBUS (Jourdain et al., 2008).

The CH<sub>4</sub> emissions input to LMDz simulations are provided by the Global Carbon Project (GCP) methane  
and include anthropogenic and biofuel emissions from EDGARv4.3.2 (Janssens-Maenhout et al., 2017),  
the mean wetland emissions from Poulter et al., (2017), fire emissions from the Global Fire Emissions  
265 Database Version 4.1 (GFED4) (Randerson et al., 2018), termite emissions as described by Saunois et al.  
(2016), geological emissions based on the spatial distribution of Etiope (2015), ocean emissions from  
Lambert and Schmidt (1993) and soil uptake from Ridgwell et al. (1999). EDGARv4.3.2 data, available

until 2012, were extrapolated from 2013 to 2016 using economical statistics according to the methodology described by Saunio et al., (2016). Anthropogenic and fire emissions vary from 2000 to 2016 while  
270 natural emissions are applied as a climatology.

The spatial distributions and annual variations of the CH<sub>4</sub> emissions during the study period are shown in Fig.1. CH<sub>4</sub> emissions range from 10 to 40 kg ha<sup>-1</sup> yr<sup>-1</sup> over most natural ecosystems and can exceed 100 kg ha<sup>-1</sup> yr<sup>-1</sup> over wetlands in Canada, South America, and Central Africa, as well as over densely  
275 populated regions such as South and East Asia. Global net CH<sub>4</sub> emissions (soil uptake included) increased by 15% from 482 Tg yr<sup>-1</sup> in 2000 to 552 Tg yr<sup>-1</sup> in 2016. Of this 70 Tg yr<sup>-1</sup> increase, 60 Tg yr<sup>-1</sup> (85%) are emissions from the Northern hemisphere, mainly contributed by livestock (18 Tg yr<sup>-1</sup>, 25%), oil and gas (16 Tg yr<sup>-1</sup>, 23%), coal burning (17 Tg yr<sup>-1</sup>, 24%) and waste (13Tg yr<sup>-1</sup>, 18%). The three emission peaks in 2002, 2006 and 2015 are driven by biomass burning. This CH<sub>4</sub> emission scenario is state-of-the-art but  
280 has not been optimized for the simulated CH<sub>4</sub> mixing ratios to fit the observations.

### 2.2.2 Model simulations

Two sets of experiments (steady-state and transient simulations) have been performed to examine the impacts of the input OH fields on the global CH<sub>4</sub> burden as well as the CH<sub>4</sub> spatial distribution and annual  
285 variation. These tests excluded the OH fields from CESM1-CAM4chem and EMAC-L47MA, since they are similar to those of CESM1-WACCM and EMAC-L90MA, respectively. We also discarded the OH fields from HadGEM3-ES and UMUKCA-UCAM because output from these two models has been supplied on too coarse vertical pressure levels. Finally, 10 different OH fields (seven from CCMI, two from LMDz-INCA and one from Transcom) were used in the two sets of simulations.

290

Initially, for each OH field described in Sect. 3, we ran 30 consecutive years of LMDz simulations (with recycled same emissions, sinks, and meteorology of the year 2000) to allow the simulation to reach a

steady-state ( $\text{CH}_4$  has an approximate lifetime of 9 years in the atmosphere). This step aims to examine the impact of the magnitude and distribution of OH on the global  $\text{CH}_4$  burden.

295

Secondly, we performed transient simulations starting from the year 2000, which are forced by time-varying OH fields as well as time-varying emissions and meteorology fields. In order to compare the impacts of the different OH fields on realistic  $\text{CH}_4$  mixing ratios, for each simulation (except the one using the OH fields from INCA NMHC), the OH field has been scaled to get the same LMDz simulated  $\text{CH}_4$  loss as the one calculated by INCA NMHC in 2000, as INCA is the OH field consistently obtained using the LMDz transport. Then a series of LMDz model simulations is conducted to investigate the impact of the various OH fields on  $\text{CH}_4$  growth rates between 2000 and 2016 as summarized in Table 2.

300

The standard simulations (Run\_standard in Table 2) using the 10 different OH fields (7 are from CCMI REF-C1), included annual variations and were performed from 2000 to 2010. Since REF-C1 experiments are only available up to 2010, the influence of OH on  $\text{CH}_4$  mixing ratios after 2010 have been tested based on alternative scenarios. First, for CCMI simulations, we tested a scenario that takes into account the annual variability from the REF-C2 experiments (Run\_REF-C2 in Table 2). Previous ACCMIP model experiments showed slightly decreasing or increasing [OH] from 2000 to 2030 according to the largest or lowest radiative forcing pathways (RCP8.5 or RCP2.6), respectively (Voulgarakis et al., 2013). Top-down approaches suggested that global OH decreased by 0.5-1% annually from 2003 to 2016 (Rigby et al., 2017; Turner et al., 2017). In order to assess the recent change in [OH], we tested two additional scenarios between 2010 and 2016: one with [OH] increase of  $+0.1\% \text{ yr}^{-1}$  (Run\_OH\_inc) according to the slightly changing of OH calculated by ACCMIP models and one with [OH] decrease of  $-1\% \text{ yr}^{-1}$  (Run\_OH\_dec) according to obviously decreasing of OH calculated by top-down approaches constrained by observations. To assess influences from OH alone, we also conducted additional simulations of the period 2000 to 2016 with annually repeated prescribed [OH] equal to the year 2000 (Run\_fix\_OH) for each OH field. The

310

315

differences between these constant OH simulations and the corresponding time-varying OH simulations indicate the impact of OH inter-annual variations and trends on atmospheric CH<sub>4</sub> changes. In addition, we conducted two simulations during 2000-2010 driven by emission inventories fixed to the year 2000 to test the influences of the emission bias on our results. The two simulations use OH fields simulated by CESM-WACCM, one with inter-annual variations of OH (Run\_fix\_emis) and the other one with OH field fixed to 2000 (Run\_fix\_emis\_OH).

### 3 Analysis of OH fields

#### 3.1 Spatial distributions of tropospheric OH

Fig. 2 shows the spatial distributions of volume-weighted tropospheric mean [OH] averaged from 2000 to 2010. Based on the 14 OH fields we have assembled, the global mean volume-weighted tropospheric [OH] vary from  $8.7 \times 10^5$  to  $12.8 \times 10^5$  molec cm<sup>-3</sup>. SOCOL, which overestimation of [OH] have been reported by Staehelin et al. (2017), simulated the highest [OH]. To better compare with previous studies, we also calculated dry air mass-weighted tropospheric mean [OH] in table 4, which vary from  $9.4 \times 10^5$  to  $14.4 \times 10^5$  molec cm<sup>-3</sup> and multi-model mean value of  $11.3 \pm 1.3 \times 10^5$  molec cm<sup>-3</sup>. The tropospheric chemical CH<sub>4</sub> lifetime of the models that provided CH<sub>4</sub> chemical loss data are  $8.7 \pm 1.1$  yr. Both the multi-model mean and the (large) range of [OH] as well as tropospheric CH<sub>4</sub> chemical lifetime are consistent with previous multi-model results given by the ACCMIP project (Naik et al., 2013; Voulgarakis et al., 2013), as well as with inversions based on MCF observations (Bousquet et al., 2005; Rigby et al., 2017). The model spread remains large as ~50% of the minimum value, as noted in previous studies (e.g. Naik et al., 2013).

Table 3 summarizes their inter-hemispheric ratios of tropospheric OH and mean values over four latitudinal bands. The inter-hemispheric ratios (N/S ratios) of CCMI and INCA OH fields are within the range of 1.2-1.5, similar to those from the ACCMIP project (Naik et al., 2013). In contrast, the TransCom

OH field has a ratio of 1.0, which is more consistent with that of MCF and  $^{14}\text{C}$  constrained OH  
345 (Brenninkmeijer et al., 1992; Krol and Lelieveld, 2003; Bousquet et al., 2005). However, as discussed by  
Spivakovsky et al. (2000), the TransCom OH field may overestimate Southern Extra-tropics OH by ~25%.  
The lower N/S ratios inferred from MCF observations are mainly due to high [OH] over the Southern  
Tropics (35% higher than Northern Tropics) (Bousquet et al., 2005). In contrast, process-based simulated  
OH is 10-26% more abundant over the Northern Tropics than over the Southern Tropics, and 35% to >  
350 90% higher over 30°N-90°N than 30°S-90°S in the CCMI models. Previous studies have attributed the  
inconsistency between the simulated and the observed OH N/S ratios to a model overestimation of O<sub>3</sub> and  
underestimation of CO over the Northern Hemisphere (Naik et al., 2013; Young et al., 2013; Strode et al.,  
2015), which also have been reported for CCMI models (Strode et al., 2016; Revell et al., 2018), as well  
as to a lack of OH recycling due to the presence of VOCs over rainforest (mainly located in the Southern  
355 Tropics) (Lelieveld et al., 2008; Archibald et al., 2011).

We further assessed the simulated OH spread by comparing the detailed spatial distributions of OH fields  
in Fig. 2 and Fig.S2. Nearly all CCMI models and two versions of the INCA model simulated high [OH]  
over eastern North American and South and East Asia, which is related to higher tropospheric O<sub>3</sub>  
360 concentrations (Cooper et al., 2014; Lu et al., 2018) and NO<sub>x</sub> emissions from human activities (Lamarque  
et al., 2010; Miyazaki et al., 2012). High [OH] over these emission hotspots dominate the aforementioned  
simulated large N/S ratio. Some models also simulated high OH values over the African savanna plains  
(MOCAGE and INCA excluded), regions with intense biomass burning (van der Werf et al., 2006) and  
soil NO<sub>x</sub> emissions (Yienger and Levy 1995; Vinken et al., 2014). The O<sub>3</sub> concentrations used to generate  
365 the TransCom OH field were larger in the Southern Tropics than in the Northern latitudes (Spivakovsky  
et al., 2000), in contrast to recent observations (Cooper et al., 2014). Therefore, TransCom shows the  
highest [OH] over the Southern Tropics during biomass burning seasons (Spivakovsky et al., 2000) and  
thus a lower N/S ratio.

370 Despite consistency on high OH values over regions influenced by human activities and biomass burning, models show the largest discrepancies over some natural ecosystem such as tropical rainforests (Fig.S2). For example, INCA, CESM, HadGEM3-Es, MRI-ESM1r1, MOCAGE and GEOSCCM simulated overall low [OH] ( $4 \times 10^5$ - $14 \times 10^5$  molec  $\text{cm}^{-3}$ ) over tropical rainforests, despite differences in details, while EMAC, CMAM, SOCOL3 and UMUKCA-UCAM simulated overall high [OH] ( $16 \times 10^5$ - more than  
375  $25 \times 10^5$  molec  $\text{cm}^{-3}$ ). Tropospheric mean [OH] over the Amazon forest show the largest variations of  $>5.0 \times 10^5$  molec  $\text{cm}^{-3}$ , count for more than 50% of the multi-model mean (Fig.S2). In a more diffuse way, high latitudes of the northern hemisphere also contribute to model spread (25-35% of the model mean, Fig. S2). Besides these, inter-model differences also exist over the open ocean (up to 25% of the model mean, Fig.S2). Most simulated OH fields show higher concentrations over continents or coastal areas due to  
380 higher precursor emissions, while MRI-ESM1r1, EMAC, and GEOSCCM also simulated high values ( $>15 \times 10^5$  molec  $\text{cm}^{-3}$ ) over the open ocean. Factors contributing to these inter-model differences are further discussed in Sect. 3.3

### 3.2 Vertical distributions

385 Figure 3 shows the vertical distribution of OH fields and Table 4 provides the volume-weighted mean [OH] averaged over the troposphere and over three pressure latitudinal intervals representing the planetary boundary layer, the mid-troposphere, and the upper troposphere (surface-750, 750-500, and 500-250 hPa, respectively). At the global scale, the mean tropospheric concentration of TransCom OH increases by a factor of nearly two from the surface ( $7 \times 10^5$  molec  $\text{cm}^{-3}$ ) to 600hPa ( $13 \times 10^5$  molec  $\text{cm}^{-3}$ ) and then  
390 decreases rapidly with altitude ( $7 \times 10^5$  molec  $\text{cm}^{-3}$  at 250hPa). UMUKA-UCAM, HadGEM3-ES, CMAM, MOCAGE, and SOCL03 on the other hand all show a continuous decrease of [OH] with altitude from the surface to the upper troposphere (e.g. the global mean concentrations of MOCAGE OH decreases from  $23.6 \times 10^5$  molec  $\text{cm}^{-3}$  at the surface to  $6.4 \times 10^5$  molec  $\text{cm}^{-3}$  at 250hPa). Other OH profiles show much



395 smaller vertical variations in the troposphere (standard deviations of mean value below 200hPa  $< 2 \times 10^5$  molec cm<sup>-3</sup>).

Model simulated OH vertical distributions can also be different over land versus ocean (Fig. 3) and between the different latitudinal bands (Fig. S3). For example, SOCOL3 [OH] continuously decreases with altitude over both, land and ocean; MOCAGE OH increases from the surface ( $14.9 \times 10^5$  molec cm<sup>-3</sup>) to 800hPa ( $18.2 \times 10^5$  molec cm<sup>-3</sup>) and then decreases over land but almost continuously decreases over the ocean; CMAM and UMUKCA-UCAM only show significant vertical variations in [OH] over land. Vertical variations of most OH fields can be attributed to mid and low latitude regions, except for those of SOCOL3 and MOCAGE, that also decrease with altitude over mid and high northern latitudes (45°N -90°N, see Fig. S3).

405

### 3.3 Factors contributing to inter-model differences

Tropospheric OH is produced primarily through the reaction of O(<sup>1</sup>D) with H<sub>2</sub>O and secondarily through the reaction of NO with HO<sub>2</sub> and RO<sub>2</sub>, and is removed primarily by reacting with CO and CH<sub>4</sub> (Logan et al., 1981). Hence, factors controlling inter-model OH discrepancies can be complex as differences in model emissions, chemistry, physics, and dynamics can together impact [OH] (Nicely et al., 2017). Here we propose a qualitative analysis focusing on both, emissions and chemical mechanisms. A more quantitative analysis would require a detailed model output of production and loss pathways and is beyond the scope of this work.

415 To analyze inter-model differences in OH vertical distributions, we compared CO, NO, and O<sub>3</sub> mixing ratios in table 5 as well as O(<sup>1</sup>D) photolysis rates and specific humidity in Table S4. The inter-model variations (calculated as standard deviation/multi-model mean) in tropospheric O(<sup>1</sup>D) photolysis rates, specific humidity, and CO mixing ratios are usually <10%-20%, while NO mixing ratios show a larger

variation of 38% (12-32pptv). MRI-ESM1r1 simulated the highest NO tropospheric mixing ratio, mainly  
420 attributable to high values above 250hPa, where OH formation is limited by H<sub>2</sub>O. In addition, MRI-  
ESM1r1 has ~20% more CO emissions than MOCAGE and GEOSCCM (Fig. S5), leading to about 10  
ppbv higher CO mixing ratios, offsetting (for [OH]) its higher NO<sub>x</sub> emissions and NO mixing ratios. The  
high NO mixing ratios near the surface and mid-troposphere simulated by SOCOL3 (48 pptv below  
750hPa and 10 pptv from 750 to 500hPa), MOCAGE (26 pptv below 750hPa and 14 pptv from 750 to  
425 500hPa) and CMAM (17 ppbv below 750hPa) are consistent with their high tropospheric and near-surface  
[OH]. Tropospheric O<sub>3</sub> can also influence primary production of OH, and tropospheric O<sub>3</sub> burden reflects  
combined effects of NO<sub>x</sub>, CO, and VOCs. The high O<sub>3</sub> over the lower troposphere simulated by SOCOL3  
and low the O<sub>3</sub> over upper troposphere simulated by MOCAGE can contribute to explain the high and  
low [OH] simulated the two models over the corresponding altitudes, respectively.

430

Lighting NO<sub>x</sub>, which are mainly emitted in the middle and upper troposphere, can contribute to inter-  
model differences in NO and OH distributions (Murray et al., 2013; 2014). We compare lighting NO<sub>x</sub>  
emissions calculated by CCMi models in Table S3. High lighting NO<sub>x</sub> emissions simulated by MRI-  
ESM1r1 above 250hPa can explain high NO mixing ratios and increasing OH with altitude over the upper  
435 troposphere for this model (Fig.3.). However, High NO mixing ratios in the lower troposphere simulated  
by MOCAGE and SOCOL3 are not corresponding to high lighting NO<sub>x</sub> emissions for these models.  
Besides emissions, previous studies have reported additional factors leading to high surface NO and NO<sub>2</sub>.  
The overestimation of NO by MOCAGE could be due to the lack of N<sub>2</sub>O<sub>5</sub> heterogeneous hydrolysis on  
tropospheric aerosol, which is an efficient sink for NO<sub>x</sub> (Teyssèdre et al., 2007). SOCOL3 does not include  
440 N<sub>2</sub>O<sub>5</sub> heterogeneous hydrolysis and also overestimates tropospheric NO production by NO<sub>2</sub> photolysis  
compared to other models, due to issues with the look-up tables used in the calculation of photolysis rates  
(Revell et al. 2018). We conclude here that physical and chemical processes related to NO production and  
loss can have a large impact on OH burden and its vertical distribution. In this context, an improved

445 representation of the partitioning between NO and other nitrogen species in the models seems of great importance to correctly simulate tropospheric [OH].

Concerning the spatial distributions, as aforementioned in Sect. 3.1, the largest model discrepancies are found over tropical rain forests. The [OH] over tropical rainforest regions are mostly sensitive to natural emissions including NO<sub>x</sub> and NMVOCs, which vary among the models. Previous studies showed that 450 [OH] is more sensitive to soil and lightning emissions than to wildfires, because the former sources only emit NO<sub>x</sub> (OH source), whereas the latter emits NO<sub>x</sub>, CO and VOCs together (OH sources and OH sinks, see Murray et al., 2014). Soil NO<sub>x</sub> emissions in CCMI models range from around 4 Tg N yr<sup>-1</sup> in MOCAGE to more than 7 Tg N yr<sup>-1</sup> in GEOSCCM and 9Tg N yr<sup>-1</sup> in CMAM (Naik et al., 2013; Yienger and Levy, 1995); Lightning NO<sub>x</sub> emissions range from 3.7-10.2 Tg yr<sup>-1</sup>(table S3). In particular, lower NO<sub>x</sub> emissions 455 over South America and Africa in MOCAGE might be linked to lower [OH] over this region (Fig. S5). Isoprene and other NMVOCs remove about 3% and 7% of tropospheric OH on a global scale, respectively (Spivakovsky et al., 2000; Murray et al., 2014) and can be more important over tropical regions with higher emission rates (Sindelarova et al., 2014). The higher [OH] over tropical rainforests simulated by CMAM and UMUKCA-UCAM may be due to a lack of or the lower OH destruction by VOCs in these 460 models. Therefore, the inter-model differences in OH spatial distributions over tropical rainforests may result from differences in natural emissions of VOC species and different related chemical reactions. The stratospheric ozone can contribute to inter-model OH discrepancies through influencing O(<sup>1</sup>D) photolysis rates. However, we find that models that simulated lower stratosphere and total ozone column are not corresponding to higher O(<sup>1</sup>D) photolysis rates and [OH] (table S5 and Fig. S4), since differences in 465 photolysis schemes coupled to CCMI models can also influence the calculation of O(<sup>1</sup>D) photolysis rates(Sukhodolov et al., 2016).

### 3.4 Inter-annual variations of OH

Figure 4 shows the time series of volume-weighted tropospheric mean [OH] from 1960 to 2010 (from  
470 REF-C1 CCM1 comparison). During this period, all OH fields show small year-to-year variations of  
1.9±1.2%, remaining within  $\pm 0.5 \times 10^5$  molec cm<sup>-3</sup>. CCM1 models simulated significantly different OH  
long-term evolutions from 1960 to 1980. For example, [OH] continuously decrease in the CMAM and  
HadGEM3-ES simulations ( $\sim -0.3 \times 10^5$  molec cm<sup>-3</sup>; -3.4%); and increase in SOCOL3 ( $\sim +0.6 \times 10^5$  molec  
475 cm<sup>-3</sup>; +4.5%), UMUKCA-UCAM ( $\sim +0.5 \times 10^5$  molec cm<sup>-3</sup>; +4.8%), and MOCAGE ( $\sim +0.5 \times 10^5$  molec cm<sup>-3</sup>;  
+4.8%) during 1960-1980, while other models show no obvious long-term trend. After 1980 (1990 for  
CMAM), all models show stabilized or slightly increasing [OH]. For our period of interest (after 2000)  
and focusing on the anomaly in [OH] compared to the 2000-2010 mean (Fig. 4b), OH year-to-year  
variations are found to be smaller than in previous decades and [OH] only increases by about  $0.1-0.3 \times 10^5$   
molec cm<sup>-3</sup> from 2000 to 2010.

480

Previous atmospheric chemistry model studies have concluded that anthropogenic activities lead to only  
a small perturbation of the OH burden, as the increased OH production tend to be compensated by an  
increased loss through reactions with CO and CH<sub>4</sub> (Lelieveld et al., 2000; Naik et al., 2013). Recent  
studies highlighted that the El Niño–Southern Oscillation can significantly contribute to the [OH] inter-  
485 annual variations (Turner et al., 2018; Rowlinson et al., 2019). By combining factors that influencing OH,  
Nicely et al. (2018) modeled a small inter-annual variability of 1.6% during 1980-2015. The year-to-year  
variations of most CCM1 and INCA OH fields are consistent with Nicely et al. (2018) but much smaller  
than the OH inter-annual variability based on MCF observations (e.g. Bousquet et al., 2005; Montzka et  
al., 2011), which can reach  $8.5 \pm 1.0\%$  from 1980 to 2000, and  $2.3 \pm 1.5\%$  from 1998 to 2007, as compared  
490 to  $2.1 \pm 0.8\%$  and  $1.0 \pm 0.5\%$  here for these two periods. As for OH trend, the ensemble of ACCMIP models  
simulated large divergent OH changes (even in their signs) from 1850 to 2000 but revealed a consistent  
and significant increase of  $3.5 \pm 2.2\%$  from 1980 to 2000 (Naik et al., 2013). Here, for the same period the  
increase of CCM1 [OH] is  $4.6 \pm 2.4\%$ , consistent with the ACCMIP project (Naik et al., 2013) and with

other atmospheric chemistry model studies (Dentener et al., 2003; John et al., 2012; Holmes et al., 2013; Dalsøren et al., 2016). The slightly increasing [OH] after 2000 inferred here as well as previous model simulations (e.g. Nicely et al., 2018) cannot help to explain stalled and renewed CH<sub>4</sub> growth during the 2000s, as opposed to the decreasing in [OH] from mid-2000s calculated by Rigby et al. (2017) and Turner et al. (2017) based on MCF observations.

We further analyzed regional [OH] trends from 2000 to 2010 in Fig. 5. Instead of dividing subdomains as Naik et al. (2013) did, we calculated the trend for each model grid-cell to identify and distinguish regions with different trends. Most models show significant positive [OH] trends over tropical regions ( $0.05\text{--}0.1 \times 10^5 \text{ molec cm}^{-3} \text{ yr}^{-1}$ ) and over East and Southeast Asia ( $>0.1 \times 10^5 \text{ molec cm}^{-3} \text{ yr}^{-1}$ ). By comparing spatial distribution of OH trend with specific humidity (Fig. S6a), NO<sub>x</sub> and CO emissions (Fig. S6b), and stratosphere O<sub>3</sub> column trend, we find that positive OH trend over tropical regions are mainly corresponding to increases in water vapor (Fig. S6a) while faster NO<sub>x</sub> emission increases ( $>5\% \text{ yr}^{-1}$ ) than CO ( $<2\% \text{ yr}^{-1}$ ) are consistent with positive OH trend over East and Southeast Asia (Fig. S6b). From 2000 to 2010, NO<sub>x</sub> emissions in the MACCity (RCP85) inventory increased by 83% over East Asia, which is much larger than the CO increase (8%) (Riahi et al., 2011). Over the rest of the extra-tropical regions such as North America and Western Europe, the models disagree on the sign of OH change. In the Southern hemisphere, where biogenic and fire emissions dominate, most OH fields do not show clear trends and the inter-model differences are even larger. For example, MOCAGE simulated and OH decrease of  $>0.1 \times 10^5 \text{ molec cm}^{-3} \text{ yr}^{-1}$  over the Amazon, South Africa, and Indonesia, whereas MRI-ESM and EMAC-L90MA simulated positive OH trends over these regions. CMAM and HadGEM3-ES show significant increasing and decreasing OH trend over the Antarctic region, respectively, consistent with the significant changes found for stratospheric O<sub>3</sub> (Fig. S6c).

In the following, we investigate how the differences in mean [OH] and variations presented in this section

affect CH<sub>4</sub> burden and its variations for the period 2000-2016.

520

## 4 Influences of OH fields on CH<sub>4</sub> simulations

### 4.1 Global total CH<sub>4</sub> burden

We now present the results based on the first set of LMDz experiments, where the LMDz model was run  
525 for 30 years recycling the year 2000 until the steady-state is reached. The simulations using the OH fields  
as given by CCMI and INCA models provide a wide range of values for the tropospheric global mean  
CH<sub>4</sub> mixing ratios (Table 6), from 1204 ppbv (SOCOL3, with a global volume-weighted tropospheric  
mean [OH] of  $12.8 \times 10^5$  molec cm<sup>-3</sup>) to 1822 ppbv (INCA NMHC-AER-S, with a global volume-  
weighted tropospheric mean [OH] of  $8.7 \times 10^5$  molec cm<sup>-3</sup>). It appears that the global CH<sub>4</sub> burden is not  
530 only sensitive to the global mean [OH], but also to its vertical distribution. Indeed, the OH radicals in the  
lower troposphere are more efficient to oxidize CH<sub>4</sub> molecules, because the CH<sub>4</sub>+OH reaction rate  
increases with temperature (Eq. 1). When considering the standard atmosphere, the reaction rate  
corresponding to the surface temperature of 288K ( $5.2 \times 10^{-15}$  s<sup>-1</sup>) is more than twice that for the 500hPa  
temperature of 253K ( $2.2 \times 10^{-15}$  s<sup>-1</sup>). Despite similar volume-weighted tropospheric mean [OH] of  $\sim 10.4$   
535  $\times 10^5$  molec cm<sup>-3</sup>, MOCAGE simulated much lower CH<sub>4</sub> mixing ratios (1275 ppbv) than CMAM (1540  
ppbv) and MRI-ESM1r1 (1639 ppbv) because of its higher near surface [OH] ( $19 \times 10^5$  molec m<sup>-3</sup>) (Table  
4). Previous studies have demonstrated that the sensitivity of CH<sub>4</sub> oxidation to lower tropical temperature  
(Spivakovsky et al., 2000; John et al., 2012), and our simulations show that 36%-46% of CH<sub>4</sub> is oxidized  
over lower tropical region (surface-750hPa, 30 °S-30 °N) (Table S6). The spatial distribution of the OH  
540 radicals also slightly influences CH<sub>4</sub> oxidation. Indeed, the [OH] of EMAC-L90MA are higher than those  
of CESM-WACCM for both, tropospheric ( $11.1 \times 10^5$  versus  $10.7 \times 10^5$  molec cm<sup>-3</sup>) and near-surface  
( $12.5 \times 10^5$  versus  $12.4 \times 10^5$  molec cm<sup>-3</sup>) means, but a slightly higher CH<sub>4</sub> burden is found for the former  
(1579 versus 1575ppbv, Table 6). This is because EMAC-L90MA simulated higher [OH] over the ocean,

while CESM-WACCM OH is more concentrated over land closer to CH<sub>4</sub> source regions. The model  
545 experiments also emphasize that volume-weighted tropospheric concentrations cannot fully indicate the  
atmospheric oxidizing efficiency for CH<sub>4</sub>, as has been discussed by Lawrence et al. (2001). Tropospheric  
mean [OH] weighted by reaction rates with CH<sub>4</sub>, which consider both temperature and CH<sub>4</sub> distributions,  
can be a better indicator for CH<sub>4</sub> oxidation (Lawrence et al., 2001).

## 550 **4.2 Impacts on CH<sub>4</sub> spatial distribution and growth rate**

In order to address the question of inter-annual variability of atmospheric CH<sub>4</sub>, we scaled each OH field  
globally to get the same CH<sub>4</sub> loss (for the year 2000) as the one obtained with INCA NMHC OH field  
(see Sect. 2.2.2). The single global scaling factor (per OH field) for the year 2000 is applied to every year  
between 2000 and 2010. As listed in Table 4, after scaling most OH fields have volume-weighted  
555 tropospheric mean concentrations closer to INCA NMHC ( $9.7 \times 10^5$  molec cm<sup>-3</sup>), within the range of 9.0-  
 $10.4 \times 10^5$  molec cm<sup>-3</sup>. One exception is MOCAGE, with tropospheric mean [OH] scaled to  $7.7 \times 10^5$  molec  
cm<sup>-3</sup>, due to its distinct vertical distribution (Sect.3.2). This scaling of OH makes it possible to start model  
experiments at the same initial CH<sub>4</sub> burden. Although slightly modifying the magnitude of the global  
mean [OH], this scaling maintained the spatial and temporal differences and trend over the 2000-2010  
560 period.

### 4.2.1 Spatial distributions of tropospheric CH<sub>4</sub> mixing ratios

We used the scaled OH fields to perform simulations between 2000 and 2010. Figure 6 shows the spatial  
distribution of tropospheric CH<sub>4</sub> mixing ratios for the simulation Run\_standard (Table. 2, driven by OH  
565 with inter-annual variations) averaged over 2000-2010. Although all simulations started from the same  
initial conditions and OH fields were scaled to give the same global CH<sub>4</sub> loss as INCA NMHC in 2000,  
LMDz simulations using the different scaled OH fields still generated a spread of tropospheric mean  
(8ppbv) and spatial distribution of CH<sub>4</sub> mixing ratios averaged during 2000-2010. Differences between

the global tropospheric mean [OH] cannot explain these differences (see Table 4). Clearly the different  
570 spatial (horizontal and vertical) and temporal variations of the OH fields (as described in Sect. 3), which  
were kept in this experiment by only scaling [OH] globally, significantly modify the simulated CH<sub>4</sub>  
mixing ratios (Table 7 and Fig. 6). OH fields with increasing trend will lead to lower LMDz simulated  
CH<sub>4</sub> mixing ratios. The LMDz simulations using the TransCom OH fields (without inter-annual  
variability) shows the highest CH<sub>4</sub> mixing ratios (1735 ppbv), while the one using the CMAM OH (with  
575 slightly increasing OH trend during the decade) shows the lowest mixing ratios (1727 ppbv).

The differences in spatial distribution of OH fields can influence LMDz simulated CH<sub>4</sub> spatial  
distributions. Looking at latitudinal CH<sub>4</sub> mixing ratios, the inter-model differences appear larger than in  
the global mean (Fig. 6 and Table 7). The model spreads of the mean CH<sub>4</sub> mixing ratios over 60°S-90°S  
580 and 60°N-90°N range from 1771 to 1794 ppbv and 1784 to 1812 ppbv, respectively. Here, we define the  
N/S gradient of CH<sub>4</sub> as the difference in mean CH<sub>4</sub> mixing ratio between the latitudinal bands 60°N -  
90°N and from 60°S - 90°S. With the TransCom OH field (N/S ratio = 1.0), the model simulated 12-43%  
larger N/S gradients of CH<sub>4</sub> (129 ppbv) than other simulations (90-115 ppbv) driven by OH fields with  
higher N/S OH ratios of 1.2-1.5. Previous model studies have attributed the overestimation of the CH<sub>4</sub>  
585 N/S ratio to an underestimation of model inter-hemispheric exchange time (e.g. Zimmermann et al., 2018).  
Our results show that uncertainties in OH distributions can also contribute to such model biases.

#### 4.2.2 Changes in CH<sub>4</sub> mixing ratios

To assess the influence of OH inter-annual variations on CH<sub>4</sub> mixing ratios, we calculated the difference  
590 in the simulated CH<sub>4</sub> between the standard run (Run\_standard) and the simulations with fixed [OH]  
(Run\_fix\_OH, Table 2). The Run\_fix\_OH simulations show that global tropospheric mean CH<sub>4</sub> mixing  
ratios increased by 75 ppbv from 2000 to 2010 (Fig. 7, black dashed lines), due to the enhanced emissions  
(Fig.1). The increase in [OH] can obviously reduce CH<sub>4</sub> growth. An increase in [OH] by  $0.1-0.3 \times 10^5$



molec cm<sup>-3</sup> (1%-3%) (Fig. 7, orange lines) during this period leads to a reduction of the CH<sub>4</sub> mixing ratios  
595 by 5-15 ppbv by 2010 (Fig. 7, blue lines). The largest reductions are found when using CESM1-WACCM  
and CMAM OH fields, given the continuous OH growth in these models. Compared to Run\_fix\_OH, we  
estimated that such reductions in CH<sub>4</sub> mixing ratios offset 7- 20% of the CH<sub>4</sub> increase driven by the rising  
CH<sub>4</sub> emissions of our scenario over the period 2000 to 2010.

600 To test whether the impacts of [OH] year-to-year variations on CH<sub>4</sub> mixing ratios the chosen emission  
scenarios, we compare the above results with that calculated by an extreme scenario where model  
simulations are driven by fixed emission (year 2000, Run\_fix\_emis and Run\_fix\_emis\_OH, table 2). With  
emissions fixed to 2000, the CH<sub>4</sub> mixing ratio increased by 2ppbv from 2000 to 2010, and increasing OH  
(CESM-WACCM OH fields) can reduce CH<sub>4</sub> mixing ratio by 13.5ppb in 2010, comparable to 13.9 ppb  
605 calculated by Run\_std and Run\_fix\_OH with CESM-WACCM OH fields. The results indicate only a  
small effect of emission scenario choices on the absolute changes of CH<sub>4</sub> mixing ratios due to OH  
variations. However, our choices have a large effect on relative change to the total modeled CH<sub>4</sub> increase.  
Indeed, if we use the emission scenarios that match observations (~+25ppbv of CH<sub>4</sub> mixing ratio increase  
from 2000-2010, Ed Dlugokencky, NOAA/ESRL, 2019) instead of ~70ppb here, the CH<sub>4</sub> mixing ratio  
610 changes due to OH can contribute to more than half (13.5-13.9ppbv versus 25ppbv) of the changes driven  
by emissions.

After 2010, CCM1 REF-C2 experiments simulated increasing, relatively stable, or decreasing OH  
variations, thus having a variable influence on CH<sub>4</sub> variations. Over the period 2011-2016, [OH]  
615 simulated by EMAC-L90MA, CESM-WACCM and CMAM stabilizes at a level  $0.2-0.4 \times 10^5$  molec cm<sup>-3</sup>  
higher than the concentrations in 2000, further reducing CH<sub>4</sub> mixing ratios by up to 20-30 ppbv in 2016  
(Fig. 7, blue lines). Other OH fields have similar concentrations over 2010-2016 as in the early 2000s  
(Fig. 7, orange lines), thus simulating CH<sub>4</sub> mixing ratios that remain close to Run\_fix\_OH with

differences less than a few +/-ppbv.

620

As large uncertainties remain regarding the inter-annual variations and trend of OH after 2010, we have tested two additional OH scenarios: Run\_OH\_inc (with an annual increase of 0.1% yr<sup>-1</sup>) and Run\_OH\_dec (with an annual decrease of 1% yr<sup>-1</sup>), to assess the uncertainty range of the impact of OH changes (the orange areas in Fig. 7) on CH<sub>4</sub> mixing ratios (the blue areas in Fig. 7). In these two scenarios, the mean [OH] of run\_OH\_dec is  $\sim 7 \times 10^5$  molec cm<sup>-3</sup> (7%) lower than run\_OH\_inc in 2016 relative to the Run\_fix\_OH . If OH decreases at 1% yr<sup>-1</sup> after 2010, by 2016, the differences in CH<sub>4</sub> mixing ratios between Run\_OH\_dec and Run\_fix\_OH range -7–30ppbv, with the lower end (-7ppbv) simulated by OH from CESM1-WACCM given its highest [OH] in 2010. On the contrary, Run\_OH\_inc simulated 3-39 ppbv lower CH<sub>4</sub> mixing ratios compared to Run\_fix\_OH (the blue areas in Fig. 7). As such, uncertainties in the OH trend can clearly lead to  $> \pm 30$  ppbv changes in CH<sub>4</sub> mixing ratios (the gray areas in Fig. 7) after only 6 years of simulations, as compared to the fix-OH case.

630

It is now interesting to compare the range of simulated [CH<sub>4</sub>] changes induced by OH scenarios to changes in surface CH<sub>4</sub> observations, in order to quantify how much of the model-observation mismatch could potentially be attributed to uncertainties in [OH] and its variability (Fig. 8). To do so, we used surface CH<sub>4</sub> observations from the National Oceanic and Atmospheric Administration (NOAA) networks and selected stations with 17 years continuous records over 2000-2016. The modeled surface CH<sub>4</sub> mixing ratios are sampled according to station locations. Since the simulated absolute CH<sub>4</sub> mixing ratios largely depend on the initial conditions and OH fields, we compared changes in the simulated and observed global CH<sub>4</sub> mixing ratios starting at the same point in 2000. The observed CH<sub>4</sub> shows zero growth between 2000 and 2006 and then increases by 5.6 ppbv yr<sup>-1</sup> between 2006 and 2012 (6.4 ppb yr<sup>-1</sup> for 2006-2010) and by 9.4 ppbv yr<sup>-1</sup> after 2012(Fig.8). In this study, we do not expect to fit these CH<sub>4</sub> trends as this inter-comparison was not conducted with a set of optimized emissions. It has already been noticed that standard

640

CH<sub>4</sub> emission inventories lead to overestimated CH<sub>4</sub> mixing ratios (e.g. Saunois et al., 2016). Indeed, neither Run\_standard nor Run\_fix\_OH simulations do capture the stagnation during 2003-2006, and overestimated surface CH<sub>4</sub> increments by 2.5-5.2 ppbv yr<sup>-1</sup> during the period 2006-2010. We define highest CH<sub>4</sub> mixing ratios simulated by different OH as CH<sub>4-H</sub>, lowest CH<sub>4</sub> mixing ratios as CH<sub>4-L</sub>, and CH<sub>4</sub> simulated by Run\_fix\_OH as CH<sub>4-fix\_OH</sub>. Based on Run\_fix\_OH, on average over 2000-2016 and depending on the OH scenario, we found that [OH] changes can emphasize the model-observation mismatch by up to 19% (mean values of  $(\text{CH}_{4\text{-H}} - \text{CH}_{4\text{-fix\_OH}}) / (\text{CH}_{4\text{-fix\_OH}} - \text{observed CH}_4)$ ) during 2000-2016), or limit the model-observation mismatch by up to 54% (mean values of  $(\text{CH}_{4\text{-fix\_OH}} - \text{CH}_{4\text{-fix\_L}}) / (\text{CH}_{4\text{-fix\_OH}} - \text{observed CH}_4)$ ) during 2000-2016) (figure 8). Such comparisons strongly suggest that a better understanding of OH inter-annual variations and trends is required in order to simulate more reliable CH<sub>4</sub> trends in atmospheric chemistry models. Atmospheric chemistry transport model (Dalsøren et al., 2016) and box model studies (Rigby et al., 2017; Turner et al., 2017) have pointed out that variations in OH can partly explain the recent CH<sub>4</sub> trends. However, current top-down estimates of CH<sub>4</sub> emissions usually assume constant [OH] (Saunois et al., 2017) and attribute the model-observation discrepancies only to surface emissions rather than changes in [OH]. Our results confirm the potentially significant role played by the still uncertain OH changes in the actual changes of methane emissions since 2000.

660

## 5 Conclusions

We have analyzed 14 OH fields (11 from CCMi experiments, 2 from INCA model simulations, 1 from TransCom) to investigate the inter-model differences in the spatial distributions and trends of tropospheric OH, and estimated the influences of OH spatio-temporal distributions on tropospheric CH<sub>4</sub> by feeding them in different simulations with LMDz offline chemistry transport model.

670 Simulated global volume-weighted tropospheric mean [OH] is within the range of  $8.7 \times 10^5$ - $12.8 \times 10^5$  molec  $\text{cm}^{-3}$ , which is consistent with the (large) multi-model range of previous estimates. CCMI and INCA models simulated larger [OH] in the Northern hemisphere than in the Southern hemisphere (N/S ratio of 1.2-1.5), with consistently high OH values over anthropogenic emission hotspots in North America, East and Southeast Asia, while TransCom OH shows a N/S ratio close to 1.0. In the vertical, TransCom OH reaches its maximum value at about 600 hPa, while CCMI and INCA OH fields either continuously decrease with altitude or show very small vertical variations in the troposphere. The factors most likely responsible for these inter-model differences include i) large NO mixing ratios leading to high surface and mid-tropospheric [OH] (Teyss re et al., 2007; Pevell et al. 2018), and ii) different natural emissions as well as VOC species and chemical mechanisms driving spatial model discrepancies over natural ecosystems.

680 Simulated OH fields show small year-to-year variations, within  $\pm 0.5 \times 10^5$  molec  $\text{cm}^{-3}$  during 1960-2010. From 2000 to 2010, year-to-year variations in OH are smaller than in previous decades and all OH fields increase by about  $0.01$ - $0.03 \times 10^5$  molec  $\text{cm}^{-3} \text{ yr}^{-1}$ . Such an increase in OH is mainly attributed to the significant positive OH trend over East and Southeast Asia ( $> 0.1 \times 10^5$  molec  $\text{cm}^{-3} \text{ yr}^{-1}$ ) in response to more OH production by  $\text{NO}_x$  than OH destruction by CO, and over tropical regions in response to increasing water vapor.

690 The inter-model differences in tropospheric OH burden generate a wide range of  $\text{CH}_4$  burdens (1204-1882ppbv) when used to simulate steady-state  $\text{CH}_4$  mixing ratios in the atmospheric chemistry model LMDz. Our findings suggest that not only different global mean [OH], but also differences in the horizontal and vertical distributions between OH fields are responsible for this range ( $\text{CH}_4$  destruction rates by OH increase with temperature).

The CH<sub>4</sub> simulations for 2000-2016 using OH with inter-annual variation show that inter-model differences of the OH N/S ratio lead to 12-43% differences in the CH<sub>4</sub> N/S gradient. For the time period  
695 2000-2010, we found that a 1%-3% increase in [OH] leads to a 5-15 ppb reduction of the CH<sub>4</sub> mixing ratio until 2010, accounting for 7-20% of the simulated emission driven CH<sub>4</sub> increase over this period. After 2010, the ensemble of OH scenarios tested here leads to differences in the CH<sub>4</sub> mixing ratio of up to 30 ppb by 2016. Comparing with surface observations, we found that [OH] changes can emphasize the model-observation mismatch by up to 19%, or fill the gap between model simulations and observations  
700 by up to 54% (Figure 8). Therefore, addressing the OH variability in CH<sub>4</sub> source inversions seems critical to avoid a wrong attribution of CH<sub>4</sub> changes to emission changes only. Future work is needed to quantify the impact of this ensemble of OH fields on CH<sub>4</sub> emissions obtained by inversion and to generate improved OH fields to be used in CH<sub>4</sub> inversion studies.

## 705 **Data Availability**

Most of the CCMI datasets are available at the Centre for Environmental Data Analysis (CEDA, at <http://data.ceda.ac.uk/badc/wcrp-ccmi/data/CCMI-1/output>), the Natural Environment Research Council's Data Repository for Atmospheric Science and Earth Observation. The output of CESM1-CAM4Chem and CESM1-WACCM for CCMI is available at <http://www.earthsystemgrid.org>. Other  
710 datasets including output of INCA model simulations and LMDz experiments can be accessed by contacting the corresponding author.

## **Author contributions**

YZ, MS, and PB designed the study, analyzed data and wrote the manuscript. BZ and XL helped with  
715 data analysis and model simulations. JC, RJ, and AS discussed the results. AB developed the LMDz code for running CH<sub>4</sub> simulations. ED provided the atmospheric in situ data. Other co-authors provided numerical model outputs. All co-authors commented on the manuscript.

## **Acknowledgements**

720 This work has been funded by the Gordon and Betty Moore Foundation through Grant GBMF5439 'Advancing Understanding of the Global Methane Cycle' and takes benefit of the expertise of the Global Carbon Project methane initiative.

We acknowledge the modelling groups for making their simulations available for this analysis, the joint WCRP SPARC/IGAC Chemistry-Climate Model Initiative (CCMI) for organising and coordinating the  
725 model data analysis activity, and the British Atmospheric Data Centre (BADC) for collecting and archiving the CCMI model output.

The EMAC simulations have been performed at the German Climate Computing Centre (DKRZ) through support from the Bundesministerium für Bildung und Forschung (BMBF). DKRZ and its scientific steering committee are gratefully acknowledged for providing the HPC and data archiving resources for  
730 this consortial project ESCiMo (Earth System Chemistry integrated Modelling).

The CESM project is supported primarily by the National Science Foundation.

Eugene Rozanov work is partially supported by Swiss National Science Foundation under grant 200020\_182239 (POLE) and the gained information will be used to improve next versions of the CCM  
SOCOL.

735 Andrea Stenke was supported by the Swiss National Science Foundation under grant 200021\_138037 (FuMES).

UMUKCA-UCAM model integrations were performed using the ARCHER UK National Supercomputing Service and MONSooN system, a collaborative facility supplied under the Joint Weather and Climate Research Programme, which is a strategic partnership between the UK Met Office and the  
740 Natural Environment Research Council.

## **Competing interests**

The authors declare that they have no conflicts of interest.

745 **References**

- Allen, D. J., and Pickering, K. E.: Evaluation of lightning flash rate parameterizations for use in a global chemical transport model, *Journal of Geophysical Research: Atmospheres*, 107, ACH 15-11-ACH 15-21, doi:10.1029/2002JD002066, 2002.
- Bednarz, E. M., Maycock, A. C., Abraham, N. L., Braesicke, P., Dessens, O., and Pyle, J. A.: Future Arctic ozone recovery: the importance of chemistry and dynamics, *Atmos. Chem. Phys.*, 16, 12159–12176, doi:10.5194/acp-16-12159-2016, 2016.
- Bousquet, P., Hauglustaine, D. A., Peylin, P., Carouge, C., and Ciais, P.: Two decades of OH variability as inferred by an inversion of atmospheric transport and chemistry of methyl chloroform, *Atmos. Chem. Phys.*, 5, 2635-2656, doi:10.5194/acp-5-2635-2005, 2005.
- 755 Archibald, A. T., Levine, J. G., Abraham, N. L., Cooke, M. C., Edwards, P. M., Heard, D. E., Jenkin, M. E., Karunaharan, A., Pike, R. C., Monks, P. S., Shallcross, D. E., Telford, P. J., Whalley, L. K., and Pyle, J. A.: Impacts of HO<sub>x</sub> regeneration and recycling in the oxidation of isoprene: Consequences for the composition of past, present and future atmospheres, *Geophysical Research Letters*, 38, L05804, doi:10.1029/2010GL046520, 2011.
- 760 Bousquet, P., Ringeval, B., Pison, I., Dlugokencky, E. J., Brunke, E. G., Carouge, C., Chevallier, F., Fortems-Cheiney, A., Frankenberg, C., Hauglustaine, D. A., Krummel, P. B., Langenfelds, R. L., Ramonet, M., Schmidt, M., Steele, L. P., Szopa, S., Yver, C., Viovy, N., and Ciais, P.: Source attribution of the changes in atmospheric methane for 2006–2008, *Atmospheric Chemistry and Physics*, 11, 3689-3700, doi:10.5194/acp-11-3689-2011, 2011.
- 765 Brenninkmeijer, C. A. M., Manning, M. R., Lowe, D. C., Wallace, G., Sparks, R. J., and Volz-Thomas, A.: Interhemispheric asymmetry in OH abundance inferred from measurements of atmospheric <sup>14</sup>CO, *Nature*, 356, doi:50, 10.1038/356050a0, 1992.
- Ciais, P., Sabine, C., Bala, G., Bopp, L., Brovkin, V., al, e., and House, J. I.: Carbon and Other Biogeochemical Cycles, in: *Climate Change 2013: The Physical Science Basis. Contribution of Working Group I to the Fifth Assessment Report of the Intergovernmental Panel on Climate Change*, Cambridge University Press, Cambridge, United Kingdom and New York, NY, USA., 2013.
- 770 Colin, P., and David, R.: Possible implications of global climate change on global lightning distributions and frequencies, *Journal of Geophysical Research: Atmospheres*, 99, 10823-10831, doi:10.1029/94JD00019, 1994.
- 775 Dee, D. P., Uppala, S. M., Simmons, A. J., Berrisford, P., Poli, P., Kobayashi, S., Andrae, U., Balmaseda, M. A., Balsamo, G., Bauer, P., Bechtold, P., Beljaars, A. C. M., van de Berg, L., Bidlot, J., Bormann, N., Delsol, C., Dragani, R., Fuentes, M., Geer, A. J., Haimberger, L., Healy, S. B., Hersbach, H., Hódin, E. V., Isaksen, I., Kållberg, P., Köhler, M., Matricardi, M., McNally, A. P., Monge-Sanz, B. M., Morcrette, J.-

- J., Park, B.-K., Peubey, C., de Rosnay, P., Tavolato, C., Thépaut, J.-N., and Vitart, F.: The ERA-Interim reanalysis: configuration and performance of the data assimilation system, *Quarterly Journal of the Royal Meteorological Society*, 137, 553-597, doi:10.1002/qj.828, 2011.
- Ed Dlugokencky, NOAA/ESRL, [www.esrl.noaa.gov/gmd/ccgg/trends\\_ch4/](http://www.esrl.noaa.gov/gmd/ccgg/trends_ch4/), 2018
- Emanuel, K. A.: A Scheme for Representing Cumulus Convection in Large-Scale Models, *Journal of the Atmospheric Sciences*, 48, 2313-2329, doi:10.1175/1520-0469(1991)048<2313:ASFRCC>2.0.CO;2, 1991.
- Cooper, O. R., Parrish, D. D., Ziemke, J., Balashov, N. V., Cupeiro, M., Galbally, I. E., Gilge, S., Horowitz, L., Jensen, N. R., Lamarque, J. F., Naik, V., Oltmans, S. J., Schwab, J., Shindell, D. T., Thompson, A. M., Thouret, V., Wang, Y., and Zbinden, R. M.: Global distribution and trends of tropospheric ozone: An observation-based review, *Elementa: Science of the Anthropocene*, 2, 000029, doi: 10.12952/journal.elementa.000029, 2014.
- Crutzen, P.: A discussion of the chemistry of some minor constituents in the stratosphere and troposphere, *Pure and Applied Geophysics*, 106, 1385-1399, doi: 10.1007/bf00881092, 1973.
- Dalsøren, S. B., Myhre, C. L., Myhre, G., Gomez-Pelaez, A. J., Sørve, O. A., Isaksen, I. S. A., Weiss, R. F., and Harth, C. M.: Atmospheric methane evolution the last 40 years, *Atmospheric Chemistry and Physics*, 16, 3099-3126, doi:10.5194/acp-16-3099-2016, 2016.
- Dentener, F., Peters, W., Krol, M., van Weele, M., Bergamaschi, P., and Lelieveld, J.: Interannual variability and trend of CH<sub>4</sub> lifetime as a measure for OH changes in the 1979–1993 time period, *Journal of Geophysical Research: Atmospheres*, 108, 4442, 10.1029/2002jd002916, 2003.
- Deushi, M. and Shibata, K.: Development of a Meteorological Research Institute chemistry-climate model version 2 for the study of tropospheric and stratospheric chemistry, *Pap. Meteorol. Geophys.*, 62, 1–46, 2011.
- EHHALT, D. H.: The atmospheric cycle of methane, *Tellus*, 26, 58-70, doi:10.1111/j.2153-3490.1974.tb01952.x, 1974.
- Etminan, M., Myhre, G., Highwood, E. J., and Shine, K. P.: Radiative forcing of carbon dioxide, methane, and nitrous oxide: A significant revision of the methane radiative forcing, *Geophysical Research Letters*, 43, 12,614-612,623, doi:10.1002/2016GL071930, 2016.
- Etioppe, G.: *Natural Gas Seepage: The Earth's Hydrocarbon Degassing*, in, Springer International Publishing, Cham, 195 pp., 2015.
- Garcia, R. R. and Boville, B. A.: Downward control of the meanmeridional circulation and temperature distribution of the polar winter stratosphere, *J. Atmos. Sci.*, 51, 2238–2245, 1994.
- Granier, C., Bessagnet, B., Bond, T., D'Angiola, A., Denier van der Gon, H., Frost, G. J., Heil, A., Kaiser, J. W., Kinne, S., Klimont, Z., Kloster, S., Lamarque, J.-F., Liousse, C., Masui, T., Meleux, F., Mieville, A., Ohara, T., Raut, J.-C., Riahi, K., Schultz, M. G., Smith, S. J., Thompson, A., van Aardenne, J., van der Werf, G. R., and van Vuuren, D. P.: Evolution of anthropogenic and biomass burning emissions of air pollutants at global and regional scales during the 1980–2010 period, *Climatic Change*, 109, 163,



- 815 doi:10.1007/s10584-011-0154-1, 2011.
- Grewe, V., Brunner, D., Dameris, M., Grenfell, J. L., Hein, R., Shindell, D., and Staehelin, J.: Origin and variability of upper tropospheric nitrogen oxides and ozone at northern mid-latitudes, *Atmospheric Environment*, 35, 3421-3433, [https://doi.org/10.1016/S1352-2310\(01\)00134-0](https://doi.org/10.1016/S1352-2310(01)00134-0), 2001.
- Guth, J., Josse, B., Maréchal, V., Joly, M., and Hamer, P.: First implementation of secondary inorganic aerosols in the MOCAGE version R2.15.0 chemistry transport model, *Geosci. Model Dev.*, 9, 137–160, doi:10.5194/gmd-9-137-2016, 2016.
- 820 Hardiman, S. C., Butchart, N., O'Connor, F. M., and Rumbold, S. T.: The Met Office HadGEM3-ES chemistry–climate model: evaluation of stratospheric dynamics and its impact on ozone, *Geosci. Model Dev.*, 10, 1209-1232, doi: 10.5194/gmd-10-1209-2017, 2017.
- 825 Hauglustaine, D. A., Hourdin, F., Jourdain, L., Filiberti, M.-A., Walters, S., Lamarque, J.-F., and Holland, E. A.: Interactive chemistry in the Laboratoire de Météorologie Dynamique general circulation model: Description and background tropospheric chemistry evaluation, *Journal of Geophysical Research: Atmospheres*, 109, doi:10.1029/2003JD003957, 2004.
- Holmes, C. D., Prather, M. J., Søvde, O. A., and Myhre, G.: Future methane, hydroxyl, and their uncertainties: key climate and emission parameters for future predictions, *Atmospheric Chemistry and Physics*, 13, 285-302, 10.5194/acp-13-285-2013, 2013.
- 830 Hourdin, F., and Armengaud, A.: The Use of Finite-Volume Methods for Atmospheric Advection of Trace Species. Part I: Test of Various Formulations in a General Circulation Model, *Monthly Weather Review*, 127, 822-837, doi:10.1175/1520-0493(1999)127<0822:tuofvm>2.0.co;2, 1999.
- 835 Hourdin, F., Mauritsen, T., Gettelman, A., Golaz, J.-C., Balaji, V., Duan, Q., Folini, D., Ji, D., Klocke, D., Qian, Y., Rauser, F., Rio, C., Tomassini, L., Watanabe, M., and Williamson, D.: The Art and Science of Climate Model Tuning, *Bulletin of the American Meteorological Society*, 98, doi:589-602, 10.1175/bams-d-15-00135.1, 2017.
- Janssens-Maenhout, G., Crippa, M., Guizzardi, D., Muntean, M., Schaaf, E., Dentener, F., Bergamaschi, P., Pagliari, V., Olivier, J. G. J., Peters, J. A. H. W., van Aardenne, J. A., Monni, S., Doering, U., and Petrescu, A. M. R.: EDGAR v4.3.2 Global Atlas of the three major Greenhouse Gas Emissions for the period 1970-2012, *Earth Syst. Sci. Data Discuss.*, 2017, 1-55, doi:10.5194/essd-2017-79, 2017.
- 840 Jourdain, L., Bekki, S., Lott, F., and Lefèvre, F.: The coupled chemistry-climate model LMDz-REPROBUS: description and evaluation of a transient simulation of the period 1980–1999, *Ann. Geophys.*, 26, 1391-1413, doi: 10.5194/angeo-26-1391-2008, 2008.
- Hegglin, M. I. and Lamarque, J.-F.: The IGAC/SPARC Chemistry-Climate Model Initiative Phase-1 (CCMI-1) model data output, NCAS British Atmospheric Data Centre, [ADD ACCESS DATE], available at:<http://catalogue.ceda.ac.uk/uuid/9cc6b94df0f4469d8066d69b5df879d5>, 2015.
- 850 Hunke, E. C. and Lipscombe, W. H.: CICE: the Los Alamos sea ice model documentation and software user's manual, Version 4.0, LA-CC-06-012, Los Alamos National Laboratory, New Mexico, 2008.
- John, J. G., Fiore, A. M., Naik, V., Horowitz, L. W., and Dunne, J. P.: Climate versus emission drivers of

- methane lifetime against loss by tropospheric OH from 1860–2100, *Atmospheric Chemistry and Physics*, 12, 12021–12036, doi:10.5194/acp-12-12021-2012, 2012.
- 855 Jöckel, P., Kerkweg, A., Pozzer, A., Sander, R., Tost, H., Riede, H., Baumgaertner, A., Gromov, S., and Kern, B.: Development cycle 2 of the Modular Earth Submodel System (MESSy2), *Geosci. Model Dev.*, 3, 717–752, doi:10.5194/gmd-3-717-2010, 2010.
- Josse, B., Simon, P., and Peuch, V.-H.: Radon global simulations with the multiscale chemistry and transport model MOCAGE, *Tellus B*, 56, 339–356, 2004.
- 860 Jöckel, P., Tost, H., Pozzer, A., Kunze, M., Kirner, O., Brenninkmeijer, C. A. M., Brinkop, S., Cai, D. S., Dyroff, C., Eckstein, J., Frank, F., Garny, H., Gottschaldt, K.-D., Graf, P., Grewe, V., Kerkweg, A., Kern, B., Matthes, S., Mertens, M., Meul, S., Neumaier, M., Nützel, M., Oberländer-Hayn, S., Ruhnke, R., Runde, T., Sander, R., Scharffe, D., and Zahn, A.: Earth System Chemistry integrated Modelling (ESCiMo) with the Modular Earth Submodel System (MESSy) version 2.51, *Geosci. Model Dev.*, 9, 1153–1200, doi:10.5194/gmd-9-1153-2016, 2016.
- 865 Jonsson, A. I., de Grandpré, J., Fomichev, V. I., McConnell, J. C., and Beagley, S. R.: Doubled CO<sub>2</sub>-induced cooling in the middle atmosphere: Photochemical analysis of the ozone radiative feedback, *J. Geophys. Res.*, 109, D24103, doi:10.1029/2004JD005093, 2004.
- Krol, M., and Lelieveld, J.: Can the variability in tropospheric OH be deduced from measurements of 1,1,1-trichloroethane (methyl chloroform)?, *Journal of Geophysical Research: Atmospheres*, 108, doi:10.1029/2002JD002423, 2003.
- 870 Lamarque, J. F., Bond, T. C., Eyring, V., Granier, C., Heil, A., Klimont, Z., Lee, D., Liousse, C., Mieville, A., Owen, B., Schultz, M. G., Shindell, D., Smith, S. J., Stehfest, E., Van Aardenne, J., Cooper, O. R., Kainuma, M., Mahowald, N., McConnell, J. R., Naik, V., Riahi, K., and van Vuuren, D. P.: Historical (1850–2000) gridded anthropogenic and biomass burning emissions of reactive gases and aerosols: methodology and application, *Atmos. Chem. Phys.*, 10, 7017–7039, doi:10.5194/acp-10-7017-2010, 2010.
- 875 Lambert, G., and Schmidt, S.: Reevaluation of the oceanic flux of methane: Uncertainties and long term variations, *Chemosphere*, 26, 579–589, doi:https://doi.org/10.1016/0045-6535(93)90443-9, 1993.
- Lawrence, M. G., Jöckel, P., and von Kuhlmann, R.: What does the global mean OH concentration tell us?, *Atmos. Chem. Phys.*, 1, 37–49, doi:10.5194/acp-1-37-2001, 2001.
- 880 Lelieveld, J., and Dentener, F. J.: What controls tropospheric ozone?, *Journal of Geophysical Research: Atmospheres*, 105, 3531–3551, doi:10.1029/1999JD901011, 2000.
- Lelieveld, J., Dentener, F. J., Peters, W., and Krol, M. C.: On the role of hydroxyl radicals in the self-cleansing capacity of the troposphere, *Atmos. Chem. Phys.*, 4, 2337–2344, doi:10.5194/acp-4-2337-2004, 2004.
- 885 Lelieveld, J., Butler, T. M., Crowley, J. N., Dillon, T. J., Fischer, H., Ganzeveld, L., Harder, H., Lawrence, M. G., Martinez, M., Taraborrelli, D., and Williams, J.: Atmospheric oxidation capacity sustained by a tropical forest, *Nature*, 452, 737–740, doi:10.1038/nature06870, 2008.
- Lelieveld, J., Gromov, S., Pozzer, A., and Taraborrelli, D.: Global tropospheric hydroxyl distribution,

- budget and reactivity, *Atmospheric Chemistry and Physics*, 16, 12477-12493, doi: 10.5194/acp-16-12477-2016, 2016.
- 890 Levy, H.: Normal Atmosphere: Large Radical and Formaldehyde Concentrations Predicted, *Science*, 173, 141-143, 10.1126/science.173.3992.141, 1971.
- Lin, X., Ciais, P., Bousquet, P., Ramonet, M., Yin, Y., Balkanski, Y., Cozic, A., Delmotte, M., Evangeliou, N., Indira, N. K., Locatelli, R., Peng, S., Piao, S., Saunois, M., Swathi, P. S., Wang, R., Yver-Kwok, C., 895 Tiwari, Y. K., and Zhou, L.: Simulating CH<sub>4</sub> and CO<sub>2</sub> over South and East Asia using the zoomed chemistry transport model LMDz-INCA, *Atmospheric Chemistry and Physics*, 18, 9475-9497, doi:10.5194/acp-18-9475-2018, 2018.
- Locatelli, R., Bousquet, P., Hourdin, F., Saunois, M., Cozic, A., Couvreux, F., Grandpeix, J. Y., Lefebvre, M. P., Rio, C., Bergamaschi, P., Chambers, S. D., Karstens, U., Kazan, V., van der Laan, S., Meijer, H. A. 900 J., Moncrieff, J., Ramonet, M., Scheeren, H. A., Schlosser, C., Schmidt, M., Vermeulen, A., and Williams, A. G.: Atmospheric transport and chemistry of trace gases in LMDz5B: evaluation and implications for inverse modelling, *Geosci. Model Dev.*, 8, 129-150, 10.5194/gmd-8-129-2015, 2015.
- Logan, J. A., Prather, M. J., Wofsy, S. C., and McElroy, M. B.: Tropospheric chemistry: A global perspective, *Journal of Geophysical Research*, 86, 7210, doi:10.1029/JC086iC08p07210, 1981.
- 905 Lu, X., Hong, J., Zhang, L., Cooper, O. R., Schultz, M. G., Xu, X., Wang, T., Gao, M., Zhao, Y., and Zhang, Y.: Severe Surface Ozone Pollution in China: A Global Perspective, *Environmental Science & Technology Letters*, 5, 487-494, doi:10.1021/acs.estlett.8b00366, 2018.
- Madec, G.: NEMO ocean engine, Institut Pierre-Simon Laplace (IPSL), France, No. 27, ISSN No. 1288-1619, 2008.
- 910 Marsh, D., Mills, M. J., Kinnison, D. E., Garcia, R. R., Lamarque, J.-F., and Calvo, N.: Climate change from 1850–2005 simulated in CESM1 (WACCM), *J. Climate*, 26, 7372–7391, doi:10.1175/JCLI-D-12-00558.1, 2013.
- Masui, T., Matsumoto, K., Hijioka, Y., Kinoshita, T., Nozawa, T., Ishiwatari, S., Kato, E., Shukla, P., Yamagata, Y., and Kainuma, M.: An emission pathway for stabilization at 6 Wm<sup>-2</sup> radiative forcing, 915 *Climatic change*, 109, 59, 2011.
- McNorton, J., Chipperfield, M. P., Gloor, M., Wilson, C., Feng, W., Hayman, G. D., Rigby, M., Krummel, P. B., and Doherty, S., Prinn, R. G., Weiss, R. F., Young, D., Dlugokencky, E., and Montzka, S. A.: Role of OH variability in the stalling of the global atmospheric CH<sub>4</sub> growth rate from 1999 to 2006, *Atmospheric Chemistry and Physics*, 16, 7943-7956, 10.5194/acp-16-7943-2016, 920 2016.
- Miyazaki, K., Eskes, H. J., and Sudo, K.: Global NO<sub>x</sub> emission estimates derived from an assimilation of OMI tropospheric NO<sub>2</sub> columns, *Atmos. Chem. Phys.*, 12, 2263-2288, doi:10.5194/acp-12-2263-2012, 2012.
- Montzka, S. A., Krol, M., Dlugokencky, E., Hall, B., Jöckel, P., and Lelieveld, J.: Small Interannual 925 Variability of Global Atmospheric Hydroxyl, *Science*, 331, 67-69, doi:10.1126/science.1197640, 2011.

- Molod, A., Takacs, L., Suarez, M., Bacmeister, J., Song, I.-S., and Eichmann, A.: The GEOS-5 Atmospheric General Circulation Model: Mean Climate and Development from MERRA to Fortuna, NASA Technical Report Series on Global Modeling and Data Assimilation, NASA TM-2012-104606, 28, 117 pp., 2012.
- 930 Molod, A., Takacs, L., Suarez, M., and Bacmeister, J.: Development of the GEOS-5 atmospheric general circulation model: evolution from MERRA to MERRA2, *Geosci. Model Dev.*, 8, 1339–1356, doi:10.5194/gmd-8-1339-2015, 2015.
- Morgenstern, O., Braesicke, P., O’Connor, F. M., Bushell, A. C., Johnson, C. E., Osprey, S. M., and Pyle, J. A.: Evaluation of the new UKCA climate-composition model – Part 1: The stratosphere, *Geosci. Model Dev.*, 2, 43–57, doi:10.5194/gmd-2-43- 2009, 2009.
- 935 Morgenstern, O., Braesicke, P., O’Connor, F. M., Bushell, A. C., Johnson, C. E., Osprey, S. M., and Pyle, J. A.: Evaluation of the new UKCA climate-composition model – Part 1: The stratosphere, *Geosci. Model Dev.*, 2, 43–57, doi:10.5194/gmd-2-43-2009, 2009.
- Morgenstern, O., Hegglin, M. I., Rozanov, E., amp, apos, Connor, F. M., Abraham, N. L., Akiyoshi, H., Archibald, A. T., Bekki, S., Butchart, N., Chipperfield, M. P., Deushi, M., Dhomse, S. S., Garcia, R. R., Hardiman, S. C., Horowitz, L. W., Jöckel, P., Josse, B., Kinnison, D., Lin, M., Mancini, E., Manyin, M. E., Marchand, M., Mar écal, V., Michou, M., Oman, L. D., Pitari, G., Plummer, D. A., Revell, L. E., Saint-Martin, D., Schofield, R., Stenke, A., Stone, K., Sudo, K., Tanaka, T. Y., Tilmes, S., Yamashita, Y., Yoshida, K., and Zeng, G.: Review of the global models used within phase 1 of the Chemistry–Climate Model Initiative (CCMI), *Geoscientific Model Development*, 10, 639-671, doi:10.5194/gmd-10-639-2017, 2017.
- 940 Murray, L. T., Mickley, L. J., Kaplan, J. O., Sofen, E. D., Pfeiffer, M., and Alexander, B.: Factors controlling variability in the oxidative capacity of the troposphere since the Last Glacial Maximum, *Atmos. Chem. Phys.*, 14, 3589-3622, doi:10.5194/acp-14-3589-2014, 2014.
- 950 Naik, V., Voulgarakis, A., Fiore, A. M., Horowitz, L. W., Lamarque, J. F., Lin, M., Prather, M. J., Young, P. J., Bergmann, D., Cameron-Smith, P. J., Cionni, I., Collins, W. J., Dals øren, S. B., Doherty, R., Eyring, V., Faluvegi, G., Folberth, G. A., Josse, B., Lee, Y. H., MacKenzie, I. A., Nagashima, T., van Noije, T. P. C., Plummer, D. A., Righi, M., Rumbold, S. T., Skeie, R., Shindell, D. T., Stevenson, D. S., Strode, S., Sudo, K., Szopa, S., and Zeng, G.: Preindustrial to present-day changes in tropospheric hydroxyl radical and methane lifetime from the Atmospheric Chemistry and Climate Model Intercomparison Project (ACCMIP), *Atmospheric Chemistry and Physics*, 13, 5277-5298, doi:10.5194/acp-13-5277-2013, 2013.
- 955 Neu, J. L., Prather, M. J., and Penner, J. E.: Global atmospheric chemistry: Integrating over fractional cloud cover, *Journal of Geophysical Research: Atmospheres*, 112, D11306, doi:10.1029/2006JD008007, 2007.
- 960 Nicely, J. M., Salawitch, R. J., Canty, T., Anderson, D. C., Arnold, S. R., Chipperfield, M. P., Emmons, L. K., Flemming, J., Huijnen, V., Kinnison, D. E., Lamarque, J.-F., Mao, J., Monks, S. A., Steenrod, S. D., Tilmes, S., and Turquety, S.: Quantifying the causes of differences in tropospheric OH within global

- models, *Journal of Geophysical Research: Atmospheres*, 122, 1983-2007, 10.1002/2016jd026239, 2017.
- 965 Nicely, J. M., Canty, T. P., Manyin, M., Oman, L. D., Salawitch, R. J., Steenrod, S. D., Strahan, S. E., and  
Strode, S. A.: Changes in Global Tropospheric OH Expected as a Result of Climate Change Over the Last  
Several Decades, *Journal of Geophysical Research: Atmospheres*, 123, 10,774-710,795,  
doi:10.1029/2018JD028388, 2018.
- Nielsen, J. E., Pawson, S., Molod, A., Auer, B., da Silva, A. M., Douglass, A. R., Duncan, B., Liang, Q.,  
Manyin, M., and Oman, L. D.: Chemical mechanisms and their applications in the Goddard Earth  
970 Observing System (GEOS) earth system model, *Journal of advances in modeling earth systems*, 9, 3019-  
3044, 2017.
- Nisbet, E. G., Manning, M. R., Dlugokencky, E. J., Fisher, R. E., Lowry, D., Michel, S. E., Myhre, C. L.,  
Platt, S. M., Allen, G., Bousquet, P., Brownlow, R., Cain, M., France, J. L., Hermansen, O., Hossaini, R.,  
Jones, A. E., Levin, I., Manning, A. C., Myhre, G., Pyle, J. A., Vaughn, B., Warwick, N. J., and White, J.  
975 W. C.: Very strong atmospheric methane growth in the four years 2014-2017: Implications for the Paris  
Agreement, *Global Biogeochemical Cycles*, 33, doi:10.1029/2018GB006009, 2019.
- O'Connor, F. M., Johnson, C. E., Morgenstern, O., Abraham, N. L., Braesicke, P., Dalvi, M., Folberth, G.  
A., Sanderson, M. G., Telford, P. J., Voulgarakis, A., Young, P. J., Zeng, G., Collins, W. J., and Pyle, J. A.:  
Evaluation of the new UKCA climatecomposition model – Part 2: The Troposphere, *Geosci. Model Dev.*,  
980 7, 41–91, doi:10.5194/gmd-7-41-2014, 2014.
- Oman, L. D., Ziemke, J. R., Douglass, A. R., Waugh, D. W., Lang, C., Rodriguez, J. M., and Nielsen, J.  
E.: The response of tropical tropospheric ozone to ENSO, *Geophys. Res. Lett.*, 38, L13706,  
doi:10.1029/2011GL047865, 2011.
- Oman, L. D., Douglass, A. R., Ziemke, J. R., Rodriguez, J. M., Waugh, D. W., and Nielsen, J. E.: The  
985 ozone response to ENSO in Aura satellite measurements and a chemistry-climate simulation, *J. Geophys.  
Res.*, 118, 965–976, doi:10.1029/2012JD018546, 2013.
- Patra, P. K., Houweling, S., Krol, M., Bousquet, P., Belikov, D., Bergmann, D., Bian, H., Cameron-Smith,  
P., Chipperfield, M. P., Corbin, K., Fortems-Cheiney, A., Fraser, A., Gloor, E., Hess, P., Ito, A., Kawa, S.  
R., Law, R. M., Loh, Z., Maksyutov, S., Meng, L., Palmer, P. I., Prinn, R. G., Rigby, M., Saito, R., and  
990 Wilson, C.: TransCom model simulations of CH<sub>4</sub> and related species: linking transport, surface flux and  
chemical loss with CH<sub>4</sub> variability in the troposphere and lower stratosphere, *Atmospheric Chemistry  
and Physics*, 11, 12813-12837, doi:10.5194/acp-11-12813-2011, 2011.
- Patra, P. K., Krol, M. C., Montzka, S. A., Arnold, T., Atlas, E. L., Lintner, B. R., Stephens, B. B., Xiang,  
B., Elkins, J. W., Fraser, P. J., Ghosh, A., Hints, E. J., Hurst, D. F., Ishijima, K., Krummel, P. B., Miller,  
995 B. R., Miyazaki, K., Moore, F. L., Mühle, J., O'Doherty, S., Prinn, R. G., Steele, L. P., Takigawa, M.,  
Wang, H. J., Weiss, R. F., Wofsy, S. C., and Young, D.: Observational evidence for interhemispheric  
hydroxyl-radical parity, *Nature*, 513, doi:219, 10.1038/nature13721, 2014.
- Pison, I., Bousquet, P., Chevallier, F., Szopa, S., and Hauglustaine, D.: Multi-species inversion of CH<sub>4</sub>,  
CO and H<sub>2</sub> emissions from surface measurements, *Atmos. Chem. Phys.*, 9, 5281-5297, doi:10.5194/acp-

- 1000 9-5281-2009, 2009.
- Poulter, B., Bousquet, P., Canadell, J. G., Ciais, P., Pregon, A., Saunois, M., Arora, V. K., Beerling, D. J., Brovkin, V., and Jones, C. D.: Global wetland contribution to 2000–2012 atmospheric methane growth rate dynamics, *Environmental Research Letters*, 12, 094013, 2017.
- Prather, M. J., Holmes, C. D., and Hsu, J.: Reactive greenhouse gas scenarios: Systematic exploration of uncertainties and the role of atmospheric chemistry, *Geophysical Research Letters*, 39, L09803, doi:10.1029/2012GL051440, 2012.
- 1005 Price, C., and Rind, D.: Modeling Global Lightning Distributions in a General Circulation Model, *Monthly Weather Review*, 122, 1930-1939, doi:10.1175/1520-0493(1994)122<1930:mglDia>2.0.co;2, 1994.
- 1010 Prinn, R. G., Huang, J., Weiss, R. F., Cunnold, D. M., Fraser, P. J., Simmonds, P. G., McCulloch, A., Harth, C., Reimann, S., Salameh, P., O'Doherty, S., Wang, R. H. J., Porter, L. W., Miller, B. R., and Krummel, P. B.: Evidence for variability of atmospheric hydroxyl radicals over the past quarter century, *Geophysical Research Letters*, 32, L07809, doi:10.1029/2004GL022228, 2005.
- Randerson, J.T., G.R. van der Werf, L. Giglio, G.J. Collatz, and P.S. Kasibhatla. 2018. Global Fire Emissions Database, Version 4.1 (GFEDv4). ORNL DAAC, Oak Ridge, Tennessee, USA. doi: <https://doi.org/10.3334/ORNLDAAC/1293>
- 1015 Revell, L. E., Tummon, F., Stenke, A., Sukhodolov, T., Coulon, A., Rozanov, E., Garny, H., Grewe, V., and Peter, T.: Drivers of the tropospheric ozone budget throughout the 21st century under the medium-high climate scenario RCP 6.0, *Atmos. Chem. Phys.*, 15, 5887–5902, doi:10.5194/acp-15-5887-2015, 2015.
- 1020 Revell, L. E., Stenke, A., Tummon, F., Feinberg, A., Rozanov, E., Peter, T., Abraham, N. L., Akiyoshi, H., Archibald, A. T., Butchart, N., Deushi, M., Jöckel, P., Kinnison, D., Michou, M., Morgenstern, O., O'Connor, F. M., Oman, L. D., Pitari, G., Plummer, D. A., Schofield, R., Stone, K., Tilmes, S., Visioni, D., Yamashita, Y., and Zeng, G.: Tropospheric ozone in CCMi models and Gaussian process emulation to understand biases in the SOCOLv3 chemistry–climate model, *Atmos. Chem. Phys.*, 18, 16155-16172, doi:10.5194/acp-18-16155-2018, 2018.
- 1025 Riahi, K., Rao, S., Krey, V., Cho, C., Chirkov, V., Fischer, G., Kindermann, G., Nakicenovic, N., and Rafaj, P.: RCP 8.5—A scenario of comparatively high greenhouse gas emissions, *Climatic Change*, 109, 33-57, 10.1007/s10584-011-0149-y, 2011.
- 1030 Ridgwell, A. J., Marshall, S. J., and Gregson, K.: Consumption of atmospheric methane by soils: A process-based model, *Global Biogeochemical Cycles*, 13, 59-70, doi:10.1029/1998GB900004, 1999.
- Rigby, M., Prinn, R. G., Fraser, P. J., Simmonds, P. G., Langenfelds, R. L., Huang, J., Cunnold, D. M., Steele, L. P., Krummel, P. B., Weiss, R. F., O'Doherty, S., Salameh, P. K., Wang, H. J., Harth, C. M., Mühle, J., and Porter, L. W.: Renewed growth of atmospheric methane, *Geophysical Research Letters*, 35, 10.1029/2008gl036037, 2008.
- 1035 Rigby, M., Montzka, S. A., Prinn, R. G., White, J. W. C., Young, D., O'Doherty, S., Lunt, M. F., Ganesan,

A. L., Manning, A. J., Simmonds, P. G., Salameh, P. K., Harth, C. M., Muhle, J., Weiss, R. F., Fraser, P. J., Steele, L. P., Krummel, P. B., McCulloch, A., and Park, S.: Role of atmospheric oxidation in recent methane growth, *Proc Natl Acad Sci U S A*, 114, 5373-5377, doi:10.1073/pnas.1616426114, 2017.

1040 Sadourny, R., and Laval, K.: January and July performances of the LMD general circulation model, *New Perspectives in Climate Modeling*, In *New Perspectives in Climate Modeling*, A.L. Berger and C. Nicolis (eds.), Elsevier Press, Amsterdam, 173-197, 1984.

Rowlinson, M. J., Rap, A., Arnold, S. R., Pope, R. J., Chipperfield, M. P., McNorton, J., Forster, P., Gordon, H., Pringle, K. J., Feng, W., Kerridge, B. J., Latter, B. L., and Siddans, R.: Impact of El Niño–Southern Oscillation on the interannual variability of methane and tropospheric ozone, *Atmos. Chem. Phys.*, 19, 8669-8686, 10.5194/acp-19-8669-2019, 2019.

1045 Sander, R., Jöckel, P., Kirner, O., Kunert, A. T., Landgraf, J., and Pozzer, A.: The photolysis module JVAL-14, compatible with the MESSy standard, and the JVal PreProcessor (JVPP), *Geosci. Model Dev.*, 7, 2653-2662, doi:10.5194/gmd-7-2653-2014, 2014.

1050 Sander, S. P., Abbatt, J., Barker, J. R., Burkholder, J. B., Friedl, R. R., Golden, D. M., Huie, R., Kurylo, M. J., Moortgat, G. K., Orkin, V. L., and Wine, P. H.: Chemical kinetics and photochemical data for use in atmospheric studies evaluation number 17, Pasadena, CA: Jet Propulsion Laboratory, National Aeronautics and Space Administration, 2011.

1055 Saunio, M., Bousquet, P., Poulter, B., Peregón, A., Ciais, P., Canadell, J. G., Dlugokencky, E. J., Etiope, G., Bastviken, D., Houweling, S., Janssens-Maenhout, G., Tubiello, F. N., Castaldi, S., Jackson, R. B., Alexe, M., Arora, V. K., Beerling, D. J., Bergamaschi, P., Blake, D. R., Brailsford, G., Brovkin, V., Bruhwiler, L., Crevoisier, C., Crill, P., Covey, K., Curry, C., Frankenberg, C., Gedney, N., Höglund-Isaksson, L., Ishizawa, M., Ito, A., Joos, F., Kim, H. S., Kleinen, T., Krummel, P., Lamarque, J. F., Langenfelds, R., Locatelli, R., Machida, T., Maksyutov, S., McDonald, K. C., Marshall, J., Melton, J. R., 1060 Morino, I., Naik, V., O'Doherty, S., Parmentier, F. J. W., Patra, P. K., Peng, C., Peng, S., Peters, G. P., Pison, I., Prigent, C., Prinn, R., Ramonet, M., Riley, W. J., Saito, M., Santini, M., Schroeder, R., Simpson, I. J., Spahni, R., Steele, P., Takizawa, A., Thornton, B. F., Tian, H., Tohjima, Y., Viovy, N., Voulgarakis, A., van Weele, M., van der Werf, G. R., Weiss, R., Wiedinmyer, C., Wilton, D. J., Wiltshire, A., Worthy, D., Wunch, D., Xu, X., Yoshida, Y., Zhang, B., Zhang, Z., and Zhu, Q.: The global methane budget 2000–2012, *Earth Syst. Sci. Data*, 8, 697-751, doi:10.5194/essd-8-697-2016, 2016.

Schultz, M. G., Heil, A., Hoelzemann, J. J., Spessa, A., Thonicke, K., Goldammer, J. G., Held, A. C., Pereira, J. M. C., and van het Bolscher, M.: Global wildland fire emissions from 1960 to 2000, *Global Biogeochemical Cycles*, 22, 10.1029/2007gb003031, 2008.

1070 Scinocca, J. F., McFarlane, N. A., Lazare, M., Li, J., and Plummer, D.: Technical Note: The CCCma third generation AGCM and its extension into the middle atmosphere, *Atmos. Chem. Phys.*, 8, 7055–7074, doi:10.5194/acp-8-7055-2008, 2008.

Sindelarova, K., Granier, C., Bouarar, I., Guenther, A., Tilmes, S., Stavrakou, T., Müller, J. F., Kuhn, U., Stefani, P., and Knorr, W.: Global data set of biogenic VOC emissions calculated by the MEGAN model

over the last 30 years, *Atmospheric Chemistry and Physics*, 14, 9317-9341, doi:10.5194/acp-14-9317-2014, 2014.

Solomon, S., Kinnison, D. E., Bandoro, J., and Garcia, R.: Simulations of polar ozone depletion: an update, *J. Geophys. Res.*, 120, 7958–7974, doi:10.1002/2015JD023365, 2015.

Spivakovsky, C. M., Logan, J. A., Montzka, S. A., Balkanski, Y. J., Foreman-Fowler, M., Jones, D. B. A., Horowitz, L. W., Fusco, A. C., Brenninkmeijer, C. A. M., Prather, M. J., Wofsy, S. C., and McElroy, M. B.: Three-dimensional climatological distribution of tropospheric OH: Update and evaluation, *Journal of Geophysical Research: Atmospheres*, 105, 8931-8980, doi:10.1029/1999jd901006, 2000.

Stenke, A., Schraner, M., Rozanov, E., Egorova, T., Luo, B., and Peter, T.: The SOCOL version 3.0 chemistry-climate model: description, evaluation, and implications from an advanced transport algorithm, *Geosci. Model Dev.*, 6, 1407–1427, doi:10.5194/gmd-6-1407-2013, 2013.

Stahelin, J., Tummon, F., Revell, L., Stenke, A., and Peter, T.: Tropospheric Ozone at Northern Mid-Latitudes: Modeled and Measured Long-Term Changes, *Atmosphere*, 8, 163, 2017.

Stohl, A., Aamaas, B., Amann, M., Baker, L. H., Bellouin, N., Berntsen, T. K., Boucher, O., Cherian, R., Collins, W., Daskalakis, N., Dusinska, M., Eckhardt, S., Fuglestedt, J. S., Harju, M., Heyes, C., Hodnebrog, Ø., Hao, J., Im, U., Kanakidou, M., Klimont, Z., Kupiainen, K., Law, K. S., Lund, M. T., Maas, R., MacIntosh, C. R., Myhre, G., Myriokefalitakis, S., Olivi é D., Quaas, J., Quennehen, B., Raut, J. C., Rumbold, S. T., Samset, B. H., Schulz, M., Seland, Ø., Shine, K. P., Skeie, R. B., Wang, S., Yttri, K. E., and Zhu, T.: Evaluating the climate and air quality impacts of short-lived pollutants, *Atmos. Chem. Phys.*, 15, 10529-10566, doi: 10.5194/acp-15-10529-2015, 2015.

Strode, S. A., Duncan, B. N., Yegorova, E. A., Kouatchou, J., Ziemke, J. R., and Douglass, A. R.: Implications of carbon monoxide bias for methane lifetime and atmospheric composition in chemistry climate models, *Atmos. Chem. Phys.*, 15, 11789-11805, doi: 10.5194/acp-15-11789-2015, 2015.

Strode SA et al. (2016) Interpreting space-based trends in carbon monoxide with multiple models *Atmos Chem Phys* 16:7285-7294 doi:10.5194/acp-16-7285-2016

Sukhodolov, T., Rozanov, E., Ball, W.T., Bais, A., Tourpali, K., Shapiro, A.I., Telford, P., Smyshlyaev, S., Fomin, B., Sander, R., Bossay, S., Bekki, S., Marchand, M., Chipperfield, M.P., Dhomse, S., Haigh, J.D., Peter, T., Schmutz, W., 2016. Evaluation of simulated photolysis rates and their response to solar irradiance variability. *Journal of Geophysical Research: Atmospheres* 121, 6066-6084.

Szopa, S., Balkanski, Y., Schulz, M., Bekki, S., Cugnet, D., Fortems-Cheiney, A., Turquety, S., Cozic, A., Déandris, C., Hauglustaine, D., Idelkadi, A., Lathi ère, J., Lefevre, F., Marchand, M., Vuolo, R., Yan, N., and Dufresne, J.-L.: Aerosol and ozone changes as forcing for climate evolution between 1850 and 2100, *Climate Dynamics*, 40, 2223-2250, doi:10.1007/s00382-012-1408-y, 2013.

Telford, P. J., Abraham, N. L., Archibald, A. T., Braesicke, P., Dalvi, M., Morgenstern, O., O'Connor, F. M., Richards, N. A. D., and Pyle, J. A.: Implementation of the Fast-JX Photolysis scheme (v6.4) into the UKCA component of the MetUM chemistry-climate model (v7.3), *Geosci. Model Dev.*, 6, 161-177, doi:10.5194/gmd-6-161-2013, 2013.



Terrenoire, E., D. A. Hauglustaine, R. Valorso, and A. Cozic, Impact of present and future aircraft NO<sub>x</sub> and aerosol emissions on atmospheric composition and radiative forcing of climate, *Atmos. Chem. Phys.* in preparation, 2019.

1115 Teyss dre, H., Michou, M., Clark, H. L., Josse, B., Karcher, F., Olivi  D., Peuch, V. H., Saint-Martin, D., Cariolle, D., Atti  J. L., N d dec, P., Ricaud, P., Thouret, V., van der A, R. J., Volz-Thomas, A., and Ch roux, F.: A new tropospheric and stratospheric Chemistry and Transport Model MOCAGE-Climat for multi-year studies: evaluation of the present-day climatology and sensitivity to surface processes, *Atmos. Chem. Phys.*, 7, 5815-5860, doi:10.5194/acp-7-5815-2007, 2007.

1120 Tilmes, S., Lamarque, J.-F., Emmons, L. K., Kinnison, D. E., Ma, P.-L., Liu, X., Ghan, S., Bardeen, C., Arnold, S., Deeter, M., Vitt, F., Ryerson, T., Elkins, J.W., Moore, F., Spackman, J. R., and Val Martin, M.: Description and evaluation of tropospheric chemistry and aerosols in the Community Earth System Model (CESM1.2), *Geosci. Model Dev.*, 8, 1395–1426, doi:10.5194/gmd-8-1395-2015, 2015.

1125 Tilmes, S., Lamarque, J.-F., Emmons, L. K., Kinnison, D. E., Marsh, D., Garcia, R. R., Smith, A. K., Neely, R. R., Conley, A., Vitt, F., Val Martin, M., Tanimoto, H., Simpson, I., Blake, D. R., and Blake, N.: Representation of the Community Earth System Model (CESM1) CAM4-chem within the Chemistry-Climate Model Initiative (CCMI), *Geosci. Model Dev.*, 9, 1853-1890, doi: <https://doi.org/10.5194/gmd-9-1853-2016>, 2016.

1130 Turner, A. J., Frankenberg, C., Wennberg, P. O., and Jacob, D. J.: Ambiguity in the causes for decadal trends in atmospheric methane and hydroxyl, *Proc Natl Acad Sci U S A*, 114, 5367-5372, doi:10.1073/pnas.1616020114, 2017.

Turner, A. J., Fung, I., Naik, V., Horowitz, L. W., and Cohen, R. C.: Modulation of hydroxyl variability by ENSO in the absence of external forcing, *Proceedings of the National Academy of Sciences*, 115, 8931-8936, 10.1073/pnas.1807532115, 2018.

1135 Turner, A. J., Frankenberg, C., and Kort, E. A.: Interpreting contemporary trends in atmospheric methane, *Proceedings of the National Academy of Sciences*, 116, 2805-2813, 10.1073/pnas.1814297116, 2019.

vanTurner, A. J., Frankenberg, C., and Kort, E. A.: Interpreting contemporary trends in atmospheric methane, *Proceedings of the National Academy of Sciences*, 116, 2805-2813, 10.1073/pnas.1814297116, 2019. der Werf, G. R., Randerson, J. T., Giglio, L., Collatz, G. J., Kasibhatla, P. S., and Arellano Jr, A. F.: Interannual variability in global biomass burning emissions from 1997 to 2004, *Atmos. Chem. Phys.*, 6, 3423-3441, 10.5194/acp-6-3423-2006, 2006.

1140 Vinken, G. C. M., Boersma, K. F., Maasakkers, J. D., Adon, M., and Martin, R. V.: Worldwide biogenic soil NO<sub>x</sub> emissions inferred from OMI NO<sub>2</sub> observations, *Atmos. Chem. Phys.*, 14, 10363-10381, doi: 10.5194/acp-14-10363-2014, 2014.

1145 Voulgarakis, A., Naik, V., Lamarque, J. F., Shindell, D. T., Young, P. J., Prather, M. J., Wild, O., Field, R. D., Bergmann, D., Cameron-Smith, P., Cionni, I., Collins, W. J., Dals ren, S. B., Doherty, R. M., Eyring, V., Faluvegi, G., Folberth, G. A., Horowitz, L. W., Josse, B., MacKenzie, I. A., Nagashima, T., Plummer, D. A., Righi, M., Rumbold, S. T., Stevenson, D. S., Strode, S. A., Sudo, K., Szopa, S., and Zeng, G.:

Analysis of present day and future OH and methane lifetime in the ACCMIP simulations, *Atmospheric Chemistry and Physics*, 13, 2563-2587, 10.5194/acp-13-2563-2013, 2013.

1150 Wang, Y., and Jacob, D. J.: Anthropogenic forcing on tropospheric ozone and OH since preindustrial times, *Journal of Geophysical Research: Atmospheres*, 103, 31123-31135, doi:10.1029/1998JD100004, 1998.

Yienger, J. J., and Levy, H.: Empirical model of global soil-biogenic NO<sub>x</sub> emissions, *Journal of Geophysical Research: Atmospheres*, 100, 11447-11464, doi:10.1029/95JD00370, 1995.

1155 Yukimoto, S., Yoshimura, H., Hosaka, M., Sakami, T., Tsujino, H., Hirabara, M., Tanaka, T. Y., Deushi, M., Obata, A., Nakano, H., Adachi, Y., Shindo, E., Yabu, S., Ose, T., and Kitoh, A.: Meteorological Research Institute Earth System Model Version 1 (MRIESM1).

van der Werf, G. R., Randerson, J. T., Giglio, L., Collatz, G. J., Mu, M., Kasibhatla, P. S., Morton, D. C., DeFries, R. S., Jin, Y., and van Leeuwen, T. T.: Global fire emissions and the contribution of deforestation, savanna, forest, agricultural, and peat fires (1997–2009), *Atmos. Chem. Phys.*, 10, 11707-11735, 10.5194/acp-10-11707-2010, 2010.

1160 Walters, D. N., Williams, K. D., Boutle, I. A., Bushell, A. C., Edwards, J. M., Field, P. R., Lock, A. P., Morcrette, C. J., Stratton, R. A., Wilkinson, J. M., Willett, M. R., Bellouin, N., Bodas-Salcedo, A., Brooks, M. E., Copestake, D., Earnshaw, P. D., Hardiman, S. C., Harris, C. M., Levine, R. C., MacLachlan, C., Manners, J. C., Martin, G. M., Milton, S. F., Palmer, M. D., Roberts, M. J., Rodríguez, J. M., Tennant, W. J., and Vidale, P. L.: The Met Office Unified Model Global Atmosphere 4.0 and JULES Global Land 4.0 configurations, *Geosci. Model Dev.*, 7, 361–386, doi:10.5194/gmd-7-361-2014, 2014.

World Meteorological Organization: Definition of the tropopause, *Bulletin of the World Meteorological Organization*, 6, 136–137, 1957.

1170 Zimmerman, P. R., Chatfield, R. B., Fishman, J., Crutzen, P. J., and Hanst, P. L.: Estimates on the production of CO and H<sub>2</sub> from the oxidation of hydrocarbon emissions from vegetation, *Geophysical Research Letters*, 5, 679-682, doi:10.1029/GL005i008p00679, 1978.

Zimmermann, P. H., Brenninkmeijer, C. A. M., Pozzer, A., Jöckel, P., Zahn, A., Houweling, S., and Lelieveld, J.: Model simulations of atmospheric methane and their evaluation using AGAGE/NOAA surface- and IAGOS-CARIBIC aircraft observations, 1997–2014, *Atmospheric Chemistry and Physics Discussions*, doi: 1-45, 10.5194/acp-2017-1212, 2018.

1180

## Tables

**Table 1.** List of CCMI models included in this study with model versions and references.<sup>1</sup>

Model	Version	References
CESM1-CAM4chem	CCMI_23	Tilmes et al.(2015, 2016)
CESM1-WACCM	CCMI_30	Solomon et al. (2015); Garcia et al. (2016); Marsh et al. (2013)
CMAM	v2.1	Jonsson et al. (2004); Scinocca et al. (2008)
EMAC(offering two resolutions: EMAC-L47MA and EMAC-L90MA)	v2.51	Jöckel et al. (2010, 2016)
GEOSCCM	v3	Molod et al. (2012, 2015); Oman et al. (2011, 2013); Nielsen et al. (2017)
HadGEM3-ES	HadGEM3 GA4.0, NEMO 3.4, CICE, UKCA, MetUM8.2	Walters et al.(2014); Madec(2008); Hunke and Lipscombe(2008); Morgenstern et al.(2009); O'Connor et al.(2004); Hardiman et al.(2017)
MOCAGE	v2.15.1	Josse et al. (2004); Guth et al. (2016)
MRI-ESM1r1	v1.1	Yukimoto et al. (2012, 2011); Deushi and Shibata (2011)
SOCOL3	v3	Revell et al. (2015); Stenke et al. (2013)
UMUKCA-UCAM	MetUM 7.3	Morgenstern et al. (2009); Bednarz et al. (2016)

<sup>1</sup> The table refers to Table 2 in Morgenstern et al. (2017)

**Table 2.** List of LMDz experiments and model setups.

	Simulation period	Inter annual variability in [OH]	Inter annual variability in CH4 emissions
Run_standard	2000-2010	2000-2010	2000-2010
Run_REF-C2	2011-2016	2010 apply inter-annual variability from REF-C2	2011-2016
Run_OH_inc	2011-2016	2010 apply annual growth rate of 1‰	2011-2016
Run_OH_dec	2011-2016	2010 apply annual decrease rate of 1‰	2011-2016
Run_fix_OH	2000-2016	Constant OH (year 2000)	2010-2016
Run_fix_emis	2000-2010	2000-2010(CESM-WACCM only)	Constant (2000)
Run_fix_emis_oh	2000-2010	Constant OH (year 2000 CESM-WACCM only)	Constant (2000)

1200

**Table 3.** Inter-hemispheric ratios (N/S) of hemispheric mean OH and volume-weighted tropospheric mean [OH] for four latitude bands (in  $10^5 \text{ molec.cm}^{-3}$ ) averaged over the years 2000 to 2010. Multi-model means and standard deviations (Mean  $\pm$  stand. dev.) are also shown.

OH fields	N/S ratio	90°S-30°S ( $10^5 \text{ molec.cm}^{-3}$ )	30°S-0° ( $10^5 \text{ molec.cm}^{-3}$ )	0°-30°N ( $10^5 \text{ molec.cm}^{-3}$ )	30°N-90°N ( $10^5 \text{ molec.cm}^{-3}$ )
<b>TransCom</b>	1.0	5.8	12.7	11.8	6.2
<b>INCA NMHC-AER-S</b>	1.3	4.7	10.6	12	7.5
<b>INCA NMHC</b>	1.2	5.7	11.9	13.4	7.8
<b>CESM1-CAM4Chem</b>	1.4	5.7	12.4	15.3	9.2
<b>CESM1-WACCM</b>	1.3	5.9	12.3	15.1	9.3
<b>CMAM</b>	1.2	5.6	13.1	14.3	8.3
<b>EMAC-L47MA</b>	1.2	6	13.5	15.6	8.4
<b>EMAC-L90MA</b>	1.2	6.3	13.8	15.7	8.6
<b>GEOSCCM</b>	1.2	6.5	14.8	16.8	9.1
<b>HadGEM3-ES</b>	1.4	4.1	10.4	12.5	8.1
<b>MOCAGE</b>	1.5	5.5	11.4	14.3	10.2
<b>MRI-ESM1r1</b>	1.2	4.7	13.7	15.3	7.3
<b>SOCOL3</b>	1.5	6.8	13.5	17.0	14.0
<b>UMUKCA-UCAM</b>	1.3	5.6	13.7	14.9	9.9
<b>Mean <math>\pm</math> stand. dev.</b>	1.3 $\pm$ 0.1	5.6 $\pm$ 0.7	12.7 $\pm$ 1.3	14.6 $\pm$ 1.6	8.9 $\pm$ 1.8

1205

**Table 4.** Global mean [OH] averaged over the troposphere and three vertical pressure levels (in  $10^5$  molec  $\text{cm}^{-3}$ ) over the years 2000 to 2010. Multi-model means and standard deviations (Mean  $\pm$  stand. dev.) are also shown.

	<b>Tp-v<sup>1</sup></b>	<b>Tp-m<sup>2</sup></b>	<b>750<sup>3</sup></b>	<b>500</b>	<b>250</b>	<b>Tp scaled<sup>4</sup></b>	<b>CH<sub>4</sub> lifetime<sup>5</sup></b>
<b>TransCom</b>	9.1	10.0	9.9	12.8	9.2	9.5	/
<b>INCA NMHC-AER-S</b>	8.7	9.4	11.3	10.4	7.8	9.3	/
<b>INCA NMHC</b>	9.7	10.4	11.8	11.4	8.9	9.7	/
<b>CESM1-CAM4Chem</b>	10.7	11.3	12.2	12.3	10.7	/	9.4 yr
<b>CESM1-WACCM</b>	10.7	11.4	12.4	12.5	10.7	9.9	9.3 yr
<b>CMAM</b>	10.4	11.3	14.3	11	10.5	9.3	9.0 yr
<b>EMAC-L47MA</b>	10.9	11.3	12.1	12	10.3	/	/
<b>EMAC-L90MA</b>	11.1	11.5	12.5	12.2	10.2	10.3	/
<b>GEOSCCM</b>	11.8	12.3	12.3	13.7	12	10.4	8.9 yr
<b>HadGEM3-ES</b>	8.8	9.9	12.7	10.8	7.7	/	/
<b>MOCAGE</b>	10.4	12.5	19	13.5	7.7	7.7	7.5 yr
<b>MRI-ESM1r1</b>	10.3	10.6	12.2	10.4	9.4	10.2	10.0 yr
<b>SOCOL3</b>	12.8	14.4	19.4	15.1	10.9	9.0	7.1 yr
<b>UMUKCA-UCAM</b>	11.0	11.9	14.9	11.7	10.5	/	/
<b>Mean <math>\pm</math> stand. Dev.</b>	10.5 $\pm$ 1.1	11.3 $\pm$ 1.3	13.4 $\pm$ 2.7	12.1 $\pm$ 1.3	9.8 $\pm$ 1.3	9.5 $\pm$ 0.8	8.7 $\pm$ 1.1 yr

<sup>1</sup> Tp-v refers to the volume-weighted tropospheric mean [OH].

<sup>2</sup> Tp-m refers to the mass-weighted tropospheric mean [OH]

<sup>3</sup> 750 refers to the volume-weighted average from the surface to 750hPa, 500 refers to the volume-weighted average from 750hPa to 500 hPa, and 250 refers to the volume-weighted average from 500 to 250hPa.

<sup>4</sup> Tp scaled refer to the volume-weighted global tropospheric mean [OH] after scaling to the same CH<sub>4</sub> loss as with INCA NMHC in 2000.

<sup>5</sup> CH<sub>4</sub> lifetime is calculated global atmospheric CH<sub>4</sub> burden divided by annual total CH<sub>4</sub> tropospheric chemical loss.

**Table 5.** Global volume-weighted mean CO, N, and O<sub>3</sub> mixing ratios averaged over the whole troposphere and three pressure altitude levels for CCM1 models over 2000 to 2010.<sup>1</sup> Multi-model means and standard deviations (Mean  $\pm$  stand. dev.) are also shown.

	<b>CO ppbv</b>				<b>NO pptv</b>				<b>O<sub>3</sub> ppbv</b>			
	750	500	250	Tp	750	500	250	Tp	750	500	250	Tp
<b>CESM1-CAM4Chem</b>	76	71	70	71	9	4	12	13	32	42	57	48
<b>CESM1-WACCM</b>	75	70	69	70	9	5	12	12	31	41	55	47

<b>CMAM</b>	77	68	64	69	17	4	17	26	34	43	60	52
<b>EMAC-L47MA</b>	85	77	70	75	8	4	11	14	38	48	63	56
<b>EMAC-L90MA</b>	84	76	69	74	8	5	11	17	38	48	61	54
<b>GEOSCCM</b>	78	74	73	74	9	5	13	13	33	43	61	49
<b>MOCAGE</b>	67	68	67	67	26	14	17	20	37	42	46	43
<b>MRI-ESM1r1</b>	93	86	83	86	10	5	20	32	36	48	67	56
<b>SOCOL3</b>	79	73	74	74	48	10	14	25	43	54	67	61
<b>Mean ±stand. dev.</b>	79±7	74±6	71±5	73±5	16±13	6±3	14±3	19±7	36±4	45±5	60±7	52±6

<sup>1</sup> HadGEM3-ES and UMUKCA-UCAM are not analyzed since model output has been regridded to too coarse vertical pressure levels.

<sup>2</sup> Tp refers to the total tropospheric average, 750 refers to the average from the surface to 750hPa, 500 refers to the average from 750hPa to 500hPa, and 250 refers to the average from 500hPa to 250hPa.

**Table 6.** Global mean tropospheric CH<sub>4</sub> mixing ratios as simulated by LMDz using different OH fields and repeating year 2000 over 30 times.

CH <sub>4</sub> mixing ratio (ppbv)			
<b>INCA NMHC-AER-S</b>	1822	<b>CESM1-WACCM</b>	1575
<b>TransCom</b>	1776	<b>CMAM</b>	1540
<b>INCA NMHC</b>	1709	<b>GEOSCCM</b>	1503
<b>MRI-ESM1r1</b>	1693	<b>MOCAGE</b>	1275
<b>EMAC-L90MA</b>	1579	<b>SOCOL3</b>	1204

**Table 7.** LMDz simulated CH<sub>4</sub> mixing ratios (in ppbv) averaged over each latitudinal band and the years 2000 to 2010 simulated from the standard experiment (Run\_standard) using different OH fields. Multi-model means and standard deviations (Mean ±stand. dev.) are also shown.

	90 °S-60 °S	60 °S-0 °	0 °-60 °N	60 °N-90 °N	N/S gradient <sup>1</sup>
<b>TransCom</b>	1683	1697	1769	1812	129
<b>INCA NMHC-AER-S</b>	1687	1698	1757	1795	108
<b>INCA NMHC</b>	1687	1700	1762	1802	115
<b>CESM1-WACCM</b>	1688	1701	1757	1794	106
<b>CMAM</b>	1682	1694	1756	1796	114
<b>EMAC-L90MA</b>	1685	1698	1759	1798	113

<b>GEOSCCM</b>	1688	1701	1764	1803	115
<b>MOCAGE</b>	1686	1699	1753	1788	102
<b>MRI-ESM1r1</b>	1691	1702	1762	1803	112
<b>SOCOL3</b>	1694	1707	1754	1784	90
<b>Mean <math>\pm</math> stand. dev.</b>	1687 $\pm$ 4	1700 $\pm$ 3	1759 $\pm$ 5	1798 $\pm$ 8	110 $\pm$ 10

<sup>1</sup> N/S gradient is defined as the difference between 60° N to 90° N and 60° S to 90° S.

1240

## Figures

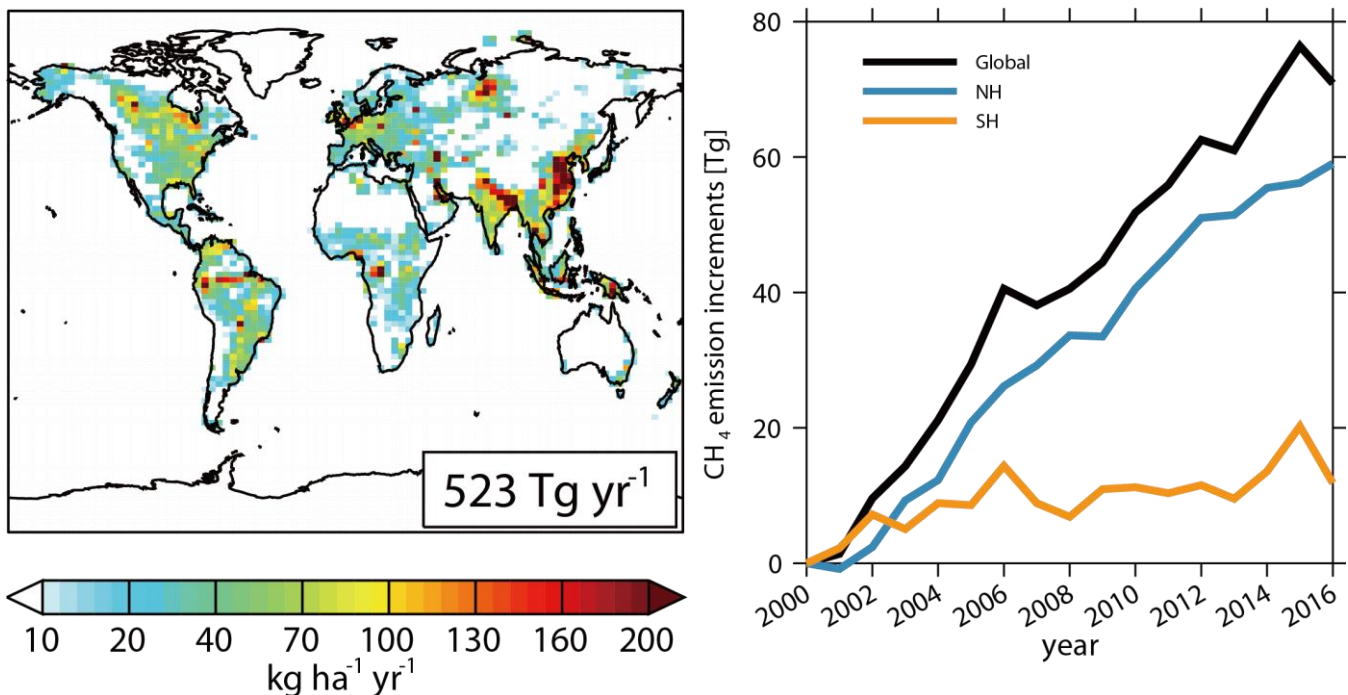


**Figure 1.** Spatial distribution of global CH<sub>4</sub> emissions averaged between 2000 and 2016 (left) and a time series of CH<sub>4</sub> emissions relative to year 2000 emissions (482 Tg CH<sub>4</sub> a<sup>-1</sup>) (right) for the globe (black line), Northern hemisphere (NH, blue line) and Southern hemisphere (SH, yellow line), respectively.

1245

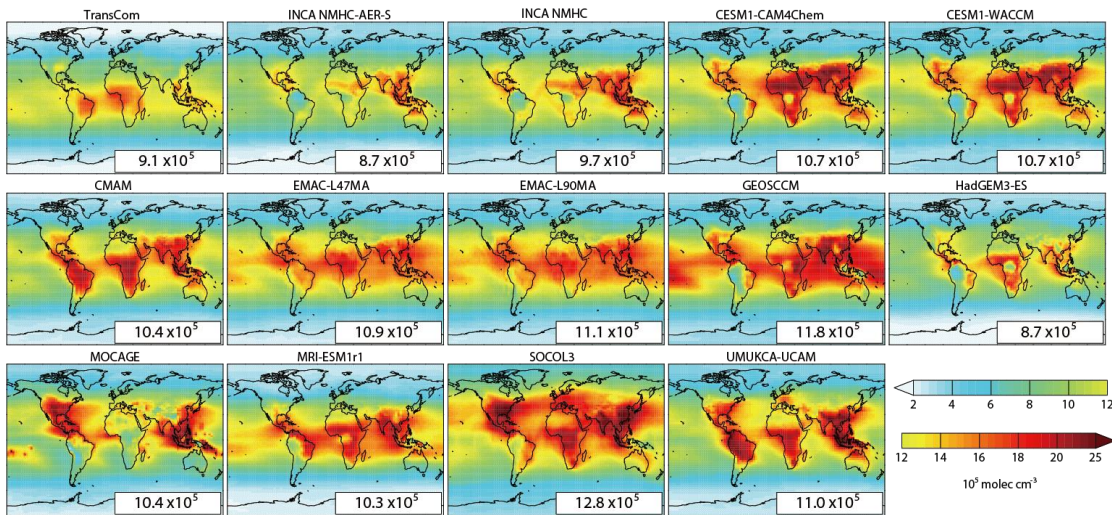


**Figure 2.** The spatial distributions of volume-weighted tropospheric mean OH fields of TransCom, INCA, and CCMI models averaged for 2000-2010. Global mean values ( $10^5 \text{ molec cm}^{-3}$ ) are shown as insets.

1250

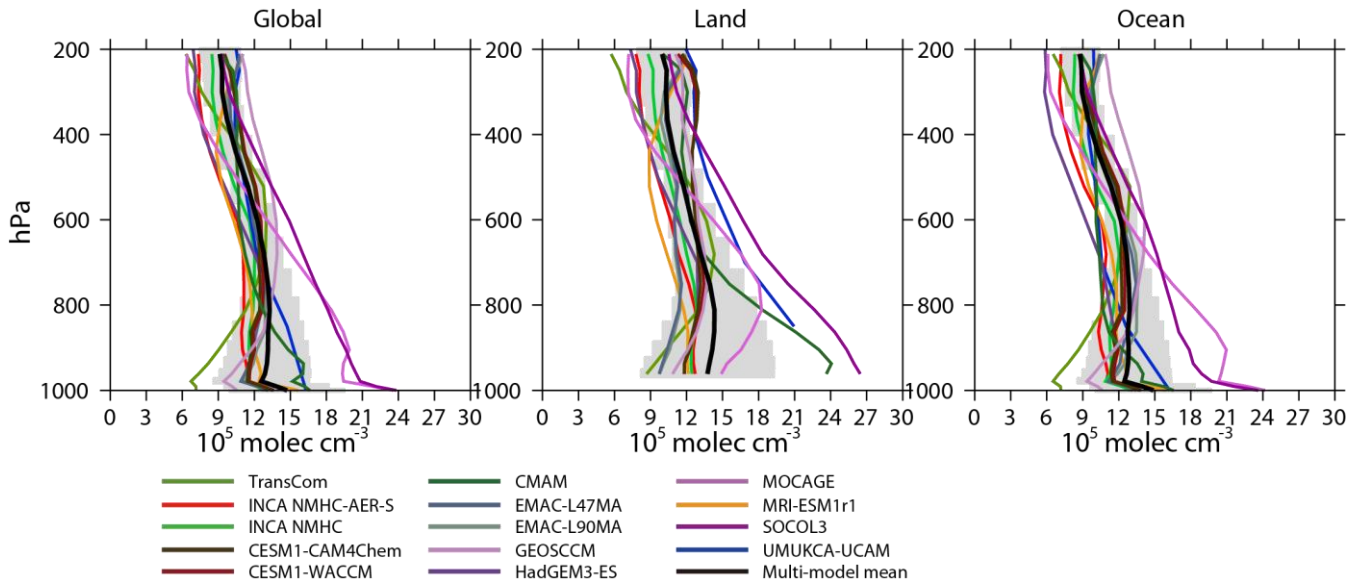
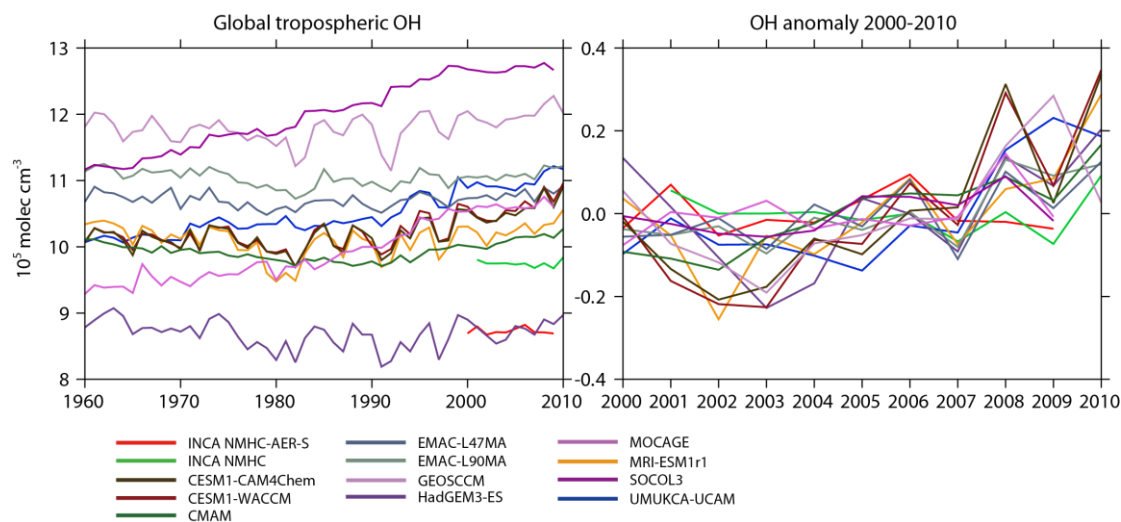


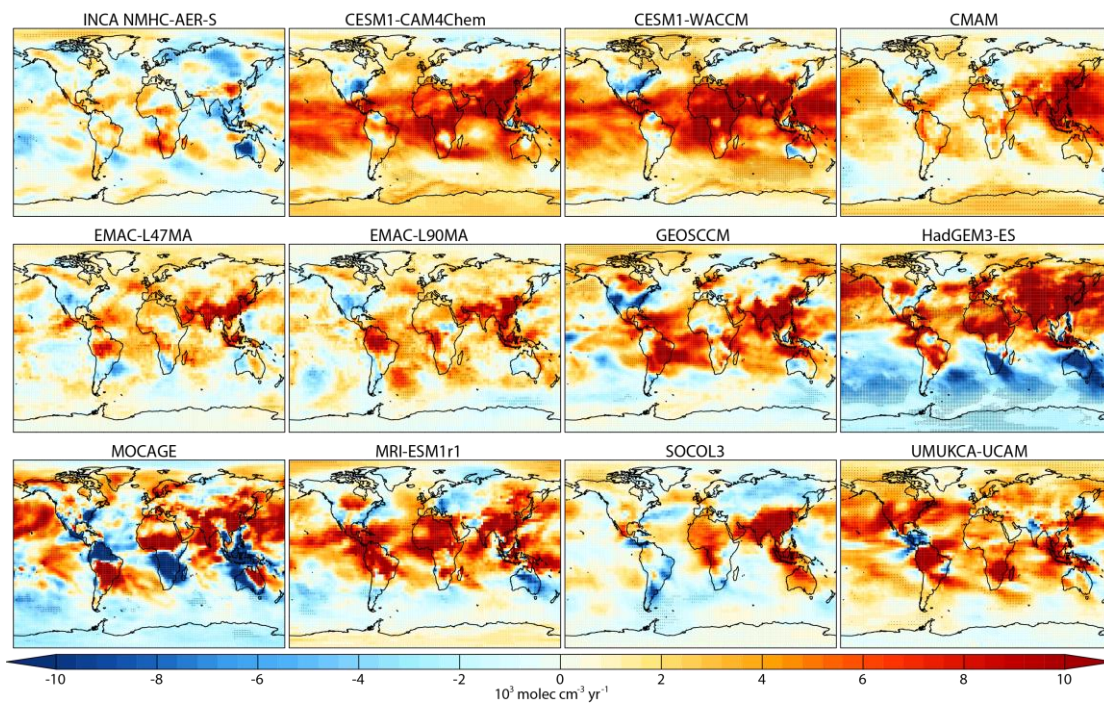
**Figure 3.** Vertical distributions of  $[\text{OH}]$  averaged over the globe (left), land (middle) and ocean (right) for 2000-2010. Color lines represent  $[\text{OH}]$  from individual model simulations, black lines represent multi-model mean values and grey shades represent the standard deviations.

1255





1260 **Figure 4.** Left: Inter-annual variations of global volume-weighted tropospheric mean [OH] from CCMI and INCA model simulations from 1960 to 2010. Right: OH anomaly during 2000-2010, in reference to the mean concentration over the period 2000-2010 for each model.



1265 **Figure 5.** Spatial distribution of tropospheric OH trends from 2000 to 2010 (in  $10^3 \text{ molec cm}^{-3} \text{ yr}^{-1}$ ). Black dots denote model grid-cells with statistically significant trends ( $p\text{-value} < 0.05$ )

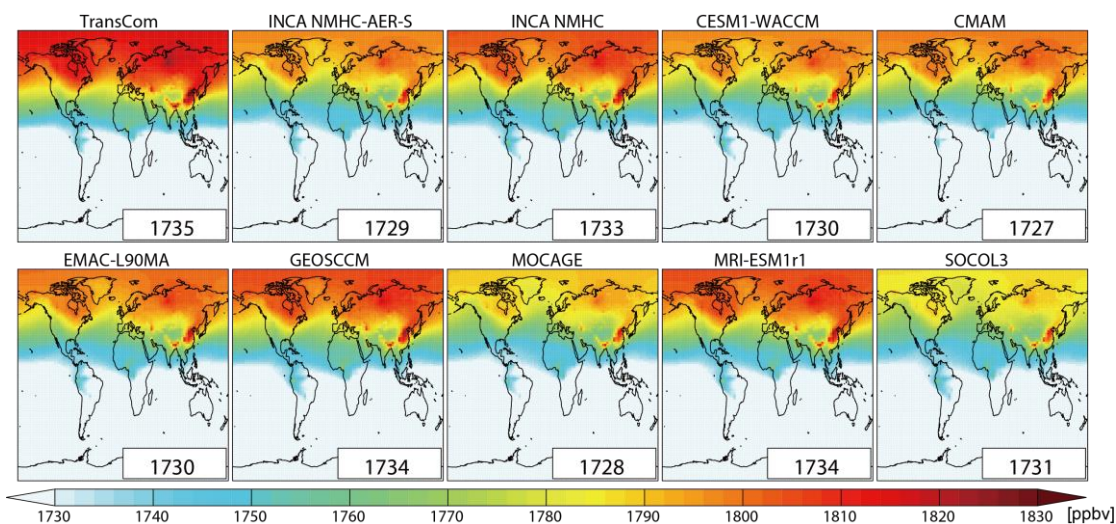


**Figure 6.** Spatial distribution of volume-weighted tropospheric mean CH<sub>4</sub> mixing ratios averaged from 2000 to 2010 as simulated by LMDz with different OH fields in the LMDz model. The global mean values in units of ppbv are shown as insets.

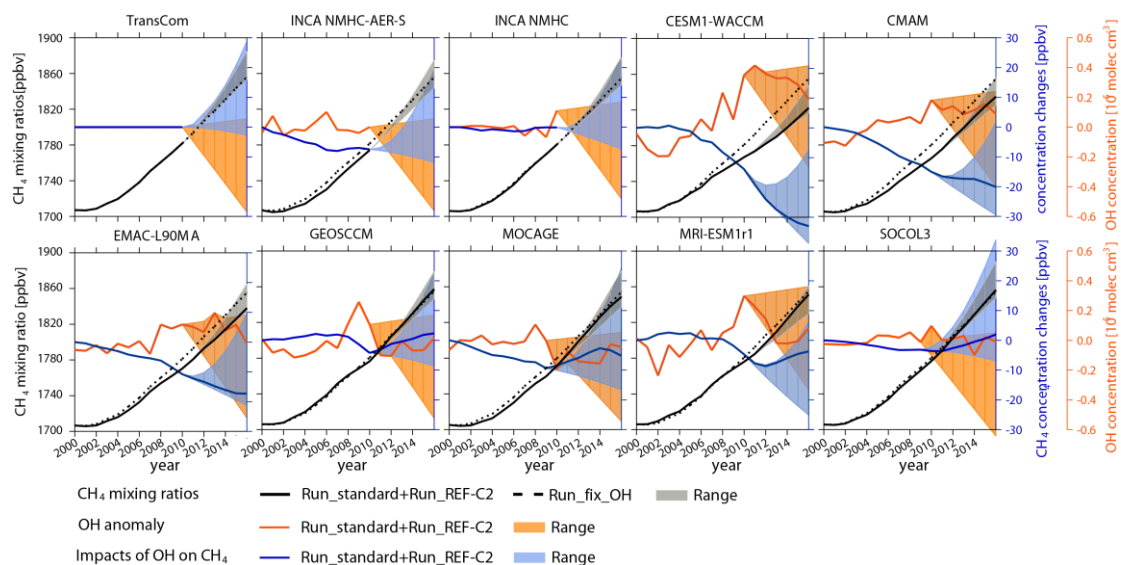


**Figure 7.** Time-series of global tropospheric CH<sub>4</sub> mixing ratios and [OH] associated with the model experiments listed in Table 2. The black lines represent the evolution of CH<sub>4</sub> mixing ratios with varying (solid lines) or with constant (dashed lines) OH. The varying OH case is obtained using OH inputs from Run\_standard from 2000 to 2010 followed by Run\_REF-C2 from 2011 to 2016 (see Table 2). The blue solid lines represent the corresponding differences between the simulations with varying OH and with

1280 constant OH. The orange solid line represents the corresponding anomalies in tropospheric [OH] (with  
the average over 2000-2010 as reference). The shaded areas correspond to the range obtained from all  
simulations over 2010-2016 (Table 2) for tropospheric CH<sub>4</sub> mixing ratios (grey), for changes in  
tropospheric CH<sub>4</sub> mixing ratios (blue) and for changes in tropospheric [OH] (orange).

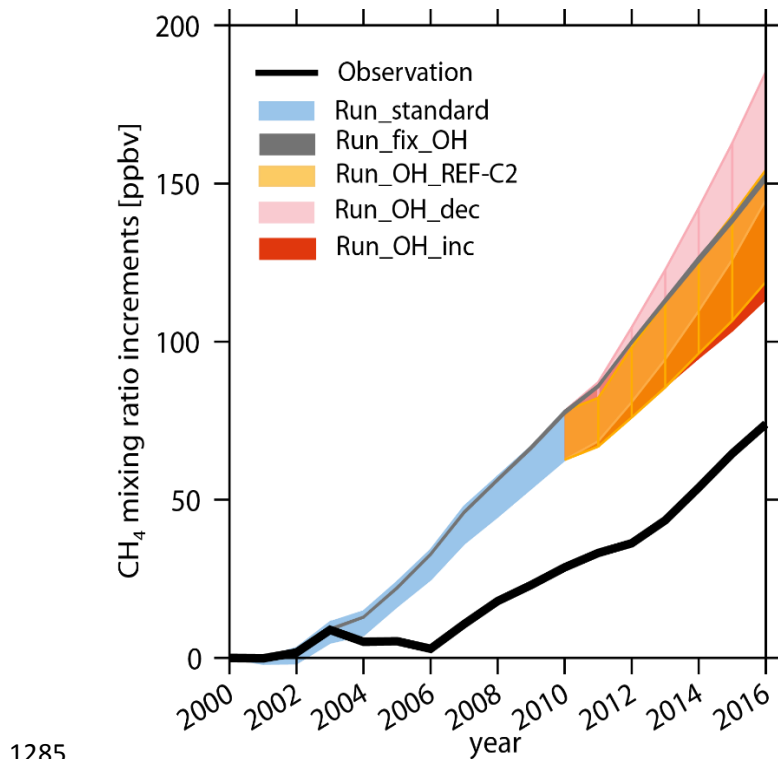


**Figure 8.** Time series of surface CH<sub>4</sub> mixing ratio increments compared to 2000 for NOAA observations (black line) and model ranges from all the LMDz experiments collected at observation sites (shades) and described in the text and in Table 2.

1290

1295